

Discriminating fluvial fans and deltas: Channel network morphometrics reflect distinct formative processes

Luke Gezovich^{1*}, Piret Plink-Björklund¹, Jack Henry^{1,2}

¹ Colorado School of Mines, Geology & Geologic Engineering, 1500 Illinois Street, Golden, CO, 80401

² Rice University, Earth, Environmental and Planetary Sciences, 6100 Main St., Houston, TX, 77005-1827

Correspondence to: Luke Gezovich (lukegezovich@mines.edu)

Abstract

Recent recognition of a new type of fluvial system – fluvial fans – introduces a fan-shaped channel network that appears similar to that of river-dominated deltas. Deltas form where rivers enter lakes and oceans, while fluvial fans are terrestrial landforms. However, fluvial fans can reach the shorelines of oceans or lakes, and in such cases the distinction between fluvial fan and river-dominated delta channel networks becomes ambiguous. We currently lack fundamental understanding of these two landforms’ morphometric differences, despite their high socioeconomic significance, vulnerability to natural hazards, and key differences in how these landforms respond to global climate change and urbanization. Here we review the relevant conceptual differences in delta and fluvial fan network morphodynamics, propose a set of quantitative morphometric criteria to distinguish fluvial fan and delta channel networks, and test these criteria on 40 deltas and 40 fluvial fans from across the world. This initial attempt to contrast and distinguish deltas and fluvial fans based on their channel network morphometrics demonstrates that quantifying channel network angles (mean of 73.8° for deltas and 55.0° for fluvial fans) and trends in normalized channel widths and lengths provide efficient criteria, but some ambiguities remain that need to be resolved in future work. This research advances our mechanistic understanding of fluvial fan and delta channel networks and the recognition of modern and ancient landforms on Earth and other planetary bodies, such as Mars and Saturn’s moon Titan.

Plain Language Summary

Fluvial fans are a newly recognized type of river system that look like river deltas, especially when they reach lakes or oceans. This study explores how to tell them apart by measuring the size and layout of channels in these fan-shaped landforms. Understanding these differences helps to predict how these landforms respond to climate change and urbanization, and to identify them on Mars and other planetary bodies.

37 1. Introduction

38 River deltas are depositional landforms that form where rivers enter lakes or oceans. They are
39 home to over half a billion people, host abundant and biodiverse ecosystems, and function as both
40 economic and agricultural hubs (Saito et al., 2007; Tejedor et al., 2015). Deltas are global change hotspots
41 highly vulnerable to urbanization and climate change, which can aggravate coastal hazards and cause sea
42 level rise (Giosan et al., 2014; Syvitski et al., 2009), and reduce sediment supply due to river damming
43 and artificial levees, causing the drowning of deltas (Blum & Roberts, 2009; Giosan et al., 2014; Nienhuis
44 et al., 2020; Paola et al., 2011; Syvitski et al., 2009). The form and function of deltas is intimately linked
45 to the evolving structure of their channel networks that determine how deltas distribute sediment and
46 nutrients (Passalacqua, 2017; Pearson et al., 2020; Tejedor et al., 2017). Delta channel network
47 morphology results from an intricate balance between sediment erosion and deposition from river, tide,
48 and wave energy fluxes. River fluxes create distributary channels and islands, tides roughen the shoreline
49 and widen the channels, and waves smooth the shoreline and decrease the number of distributary channels
50 (Broaddus et al., 2022; Galloway, 1975; Nienhuis et al., 2015, 2018; Paniagua-Arroyave & Nienhuis,
51 2024; Vulis et al., 2023). Deltas dominated by river energy fluxes (river-dominated deltas) (Broaddus et
52 al., 2022; Galloway, 1975; Nienhuis et al., 2015, 2018; Paniagua-Arroyave & Nienhuis, 2024; Vulis et
53 al., 2023) characteristically form fan-shaped landforms with complex distributary channel networks (Fig.
54 1). In these deltas, channel network topology is defined by mouth bar deposition and consequent
55 distributary channel bifurcation (Bates, 1953; Edmonds & Slingerland, 2007; Wright, 1977).

56 Fluvial fans are another type of fan-shaped landform with channel networks that share
57 morphological similarities with the river-dominated delta channel networks (Fig. 2). Fluvial fans are a
58 relatively newly acknowledged type of fluvial landform (Ventra & Clarke, 2018; Weissman et al., 2010),
59 which forms via river avulsions or “channel jumps” across low-gradient floodplains (Chakraborty et al.,
60 2010; Martin & Edmonds, 2023; North & Warwick, 2007). Rivers have been traditionally regarded as
61 sediment transfer or bypass zones in source-to-sink systems (Allen, 2008; Fielding et al., 2012), whereas
62 fluvial fans are net depositional and build significant stratigraphic thicknesses (Chakraborty et al., 2010;
63 Moscariello, 2018; Weissmann et al., 2015). Fluvial fans are also called “wet” fluvial-dominated alluvial
64 fans (Schumm, 1977), megafans (Singh et al., 1993), or distributive fluvial systems (DFS) (Weissman et
65 al., 2010). Fluvial fans are distinct landforms from alluvial fans – which form by a combination of
66 gravitational and streamflow processes, feature steep gradients (typically 2–12°), and have a relatively
67 small radius typically less than 10 km (Blair & McPherson, 1994; Moscariello, 2018). Fluvial fans form
68 some of the largest terrestrial landforms on Earth (10^3 – 10^5 km² in surface area) (Horton & Decelles, 2001;
69 Leier et al., 2005) and have low gradients (0.0018–1.5°) (Hartley et al., 2010). Fluvial fans are abundant

70 across Earth, and they form in diverse climatic and tectonic settings (Hartley et al., 2010; Ventra &
71 Clarke, 2018; Weissmann et al., 2010).

72 Like deltas, fluvial fans are home to hundreds of millions of people, and these highly dynamic
73 landforms are critical for their livelihood – supporting agriculture, fisheries, and freshwater access. They
74 also experience catastrophic floods; for example, the Kosi fluvial fan floods have led to large numbers of
75 casualties and displaced populations (Sinha, 2009; Syvitski & Brakenridge, 2013). While fluvial fans are
76 terrestrial landforms, they can reach the shorelines of oceans (Fig. 2b) or lakes (Figs. 2a, 2d and 2i). In
77 such cases the distinction between fluvial fan and river-dominated delta channel networks becomes
78 ambiguous, while wave- and tide-dominated deltas have distinctly recognizable morphologies (Broaddus
79 et al., 2022; Galloway, 1975; Nienhuis et al., 2015; 2018; Paniagua-Arroyave & Nienhuis, 2024; Vulis et
80 al., 2023). We currently lack quantitative morphometric criteria for distinguishing river-dominated delta
81 and fluvial fan channel networks, despite their socioeconomic significance, key differences in their
82 natural hazard vulnerabilities, and in how they respond to global change.

83 Numerous fan-shaped landforms with channel networks have also been identified on other planetary
84 bodies such as Mars (Malin & Edgett, 2015; Ori et al., 2000; Wood, 2006) and Saturn’s moon Titan
85 (Radebaugh et al., 2018; Wall et al., 2010; Witek & Czechowski, 2015). Deltas on planetary bodies are
86 important indicators of paleo-shorelines and have been utilized to reconstruct the shorelines and water
87 levels of ancient lakes and oceans on Mars (Di Achille & Hynek, 2010). However, Martian paleo-ocean
88 shoreline reconstructions have so far yielded mixed results (De Toffoli et al., 2021). This discrepancy
89 could perhaps arise because shoreline-bound deltas have not been effectively distinguished from fluvial
90 fans on Mars, which may form thousands of kilometers inland from shorelines (Bramble et al., 2019;
91 Limaye et al., 2023; Tebolt & Goudge, 2022). Deltas also offer attractive targets for mission sites in
92 search of life due to their habitability and high biosignature preservation potential, as exemplified by the
93 selection of Jezero Crater for NASA’s *Perseverance* rover, *Ingenuity* helicopter, and future Mars Sample
94 Return mission (Farley et al., 2020). Distinguishing deltaic and fluvial fan paleo-channel networks on
95 other planetary bodies is even more ambiguous, especially if the lakes and oceans are no longer present.

96 Over time, the accumulation of biogenic and sedimentary materials distributed via channel networks
97 contributes to the construction of stratigraphy. Fluvial fans and deltas are both net depositional systems
98 characterized by spatially diminishing water surface slopes that reduce sediment transport capacity,
99 thereby producing spatiotemporal convergence and deposition of sediment (Ganti et al., 2014).

100 Consequently, in addition to their socioeconomic significance, both landforms significantly contribute to
101 the stratigraphic record, and their deposits can be used to decipher past environmental conditions. High
102 deposition rates in fluvial fans and deltas promote the preservation of environmental change signals in the
103 sedimentary record (Trampush & Hajek, 2017). Similar to modern river-dominated deltas and fluvial

104 fans, we lack morphometric criteria to distinguish these two fan-shaped channel networks in the
105 sedimentary record, such as in seismic datasets.

106 This study is motivated by developing quantitative morphometric distinction criteria for fluvial fan
107 and river-dominated delta channel networks. Prior work has established quantitative morphological
108 criteria for describing deltaic channel networks and linked these characteristics to theory (Chen et al.,
109 2021; Coffey & Shaw, 2017; Edmonds et al., 2011; Edmonds & Slingerland, 2007; Fagherazzi et al.,
110 2015; Ke et al., 2019; Passalacqua, 2017; Pearson et al., 2020; Tejedor et al., 2015, 2017). However, there
111 are no existing quantitative criteria to characterize fluvial fan channel networks or to differentiate the two
112 landforms. To develop such criteria, we review the relevant conceptual differences in delta and fluvial fan
113 network morphodynamics, propose quantitative morphometric criteria to distinguish fluvial fan and delta
114 channel networks, and test these criteria on 40 deltas and 40 fluvial fans (Supplementary Data) from
115 across the globe (Fig. 3). We test the robustness of the approach by analyzing differences in channel
116 network morphometrics concerning the size and gradient of the systems, lake versus ocean terminations
117 and tide versus wave influences in deltas, and fan termination styles in fluvial fans. We assess how
118 effectively the proposed methods distinguish fluvial fans from river-dominated deltas and examine why
119 this distinction matters under global change. This work serves to improve our mechanistic understanding
120 of fluvial fan and delta evolution, and their accurate recognition on Earth, other planetary bodies, and in
121 the sedimentary record.

122 **2. Delta and Fluvial Fan Channel Network Morphodynamics**

123 The nature of channel networks is dependent on distinct morphodynamic processes responsible for
124 their formation (Edmonds & Slingerland, 2007; Fagherazzi et al., 2015; Tejedor et al., 2015). Below we
125 analyze differences in delta and fluvial fan morphodynamics and review existing morphometric criteria
126 for quantifying deltaic distributary channel networks. Our review is not comprehensive; rather, it focuses
127 on the specific processes that govern the formation of the morphometric characteristics that we can then
128 use for distinction of these two landforms, namely channel network angles, and downstream changes in
129 channel widths and lengths. There are other important characteristics of deltaic channel networks, linked
130 to water and sediment discharge distribution, entropy, and connectivity (Chen et al., 2021; Ke et al., 2019;
131 Passalacqua, 2017; Pearson et al., 2020; Tejedor et al., 2015, 2017). These aspects are not considered in
132 this review, because they are outside the scope of this study that seeks to distinguish deltaic and fluvial
133 fan channel networks using easily applicable morphometric criteria that can be used for both deltaic and
134 fluvial fan networks.

135 **2.1 River Deltas**

136 Deltas (Fig. 1) form only where a river enters a standing body of water. Here, the transport capacity
137 of the turbulent jet decreases, and the “parent” stream jet flow experiences both lateral and bed friction,

138 causing the flow to decelerate and rapidly expand laterally (Bates, 1953; Edmonds & Slingerland, 2007;
139 Jerolmack & Swenson, 2007; Wright, 1977). As a result, the transport capacity of the turbulent jet
140 decreases and sediment is deposited as a mouth bar basinward of the river mouth (Edmonds &
141 Slingerland, 2007). The process of mouth bar deposition and growth eventually leads to the downstream
142 branching, or *bifurcation*, of a single (parent) channel into two daughter channels (Axelsson, 1967;
143 Coffey & Shaw, 2017; Edmonds & Slingerland, 2007) (Fig. 4a). These daughter channels are separated
144 by an island or shallow bay where sediment transport is significantly reduced or nonexistent, and flow is
145 unchanneled (Coffey & Shaw, 2017). Mouth bar deposition and resultant channel bifurcation repeat
146 multiple times, leading to the seaward advancement of the shoreline and the construction of a delta
147 distributary channel network (Edmonds & Slingerland, 2007; Olariu & Bhattacharya, 2006) (Fig. 4a).

148 Deltas also experience channel avulsions or “channel jumps” at the lobe-level (Slingerland & Smith,
149 2004). These deltaic avulsions occur within a region of high-water surface slope variability caused by
150 backwater hydrodynamics that are characterized by spatial flow deceleration and deposition during low
151 flows, and flow acceleration and bed scour with high flows (Brooke et al., 2022; Chatanantavet et al.,
152 2012; Chatanantavet & Lamb, 2014). As the backwater zone sets the location for avulsion in deltas
153 (Chatanantavet et al., 2012), they are strongly controlled by hydrodynamics in their receiving basin, like
154 mouth-bar-driven bifurcations. As a result, the delta lobe size is generally consistent and the lobe avulsion
155 node migrates downstream commensurate with shoreline progradation (Ganti et al., 2014), as influenced
156 by flood frequency, sediment supply, or sea-level rise (Brooke et al., 2022). These avulsions episodically
157 rearrange the depocenter at the delta lobe scale, whereas the substantially more frequent mouth-bar-driven
158 bifurcations generate the topology of the delta distributary channel networks (Bentley et al., 2016;
159 Edmonds & Slingerland, 2007).

160 Resultant delta channel networks have a specific angle at which distributary channels bifurcate (Fig.
161 4a) (Coffey & Shaw, 2017), because a mouth-bar-driven bifurcation will grow toward an equilibrium
162 angle of 72° to maximize flux at the two channel tips (Coffey & Shaw, 2017; Devauchelle et al., 2012; Ke
163 et al., 2019; Mahon et al., 2024). First described in tributary networks, this theoretical angle arises from
164 diffusive groundwater flow (Devauchelle et al., 2012). Testing of this concept reports mouth-bar-driven
165 bifurcation angles of $70.4^\circ \pm 2.6^\circ$ ($n = 9$) in natural deltas (Coffey & Shaw, 2017), and $68.3^\circ \pm 8.7^\circ$ ($n =$
166 21) (Coffey & Shaw, 2017) and $74.1^\circ \pm 7.7^\circ$ ($n = 13$) (Federici & Paola, 2003) in experimental deltas.

167 Deltaic channel networks tend to consistently self-organize (Edmonds et al., 2011; Fagherazzi, 2008)
168 and exhibit a theoretical fractal pattern of decreasing channel widths and lengths associated with
169 increasing bifurcation order (Edmonds et al., 2011; Edmonds & Slingerland, 2007; Hariharan et al., 2022;
170 Seybold et al., 2017; Wolinsky et al., 2010) (Fig. 4a). Edmonds & Slingerland, (2007) show that channel
171 width trends align with hydraulic geometric scaling: as the discharge of a parent channel divides into the

172 discharge for two resultant daughter channels, the daughter channel dimensions decrease as they scale
173 with bankfull discharge. Channel lengths decrease downstream with each successive bifurcation because
174 the jet momentum flux and consequent average grain transport distance decrease downstream, causing
175 new mouth bar deposition and accompanying bifurcations to occur closer to the previous bifurcation node
176 for a given channel (Edmonds & Slingerland, 2007) (Figs. 4a).

177 The nature of delta channel networks is further affected by waves and tides (Broaddus et al., 2022;
178 Geleynse et al., 2011; Jerolmack & Swenson, 2007) where the relative strength of river, wave, and tide
179 processes determines whether deltas are river, wave, or tide dominated (Galloway, 1975; Nienhuis et al.,
180 2015, 2018; Paniagua-Arroyave & Nienhuis, 2024; Vulis et al., 2023). Since wave- and tide-*dominated*
181 deltas exhibit distinct morphologies from river-dominated delta and fluvial fan channel networks, they are
182 not considered in this study (See Methods for more information on classification).

183
184
185
186
187
188
189
190
191
192
193
194
195
196

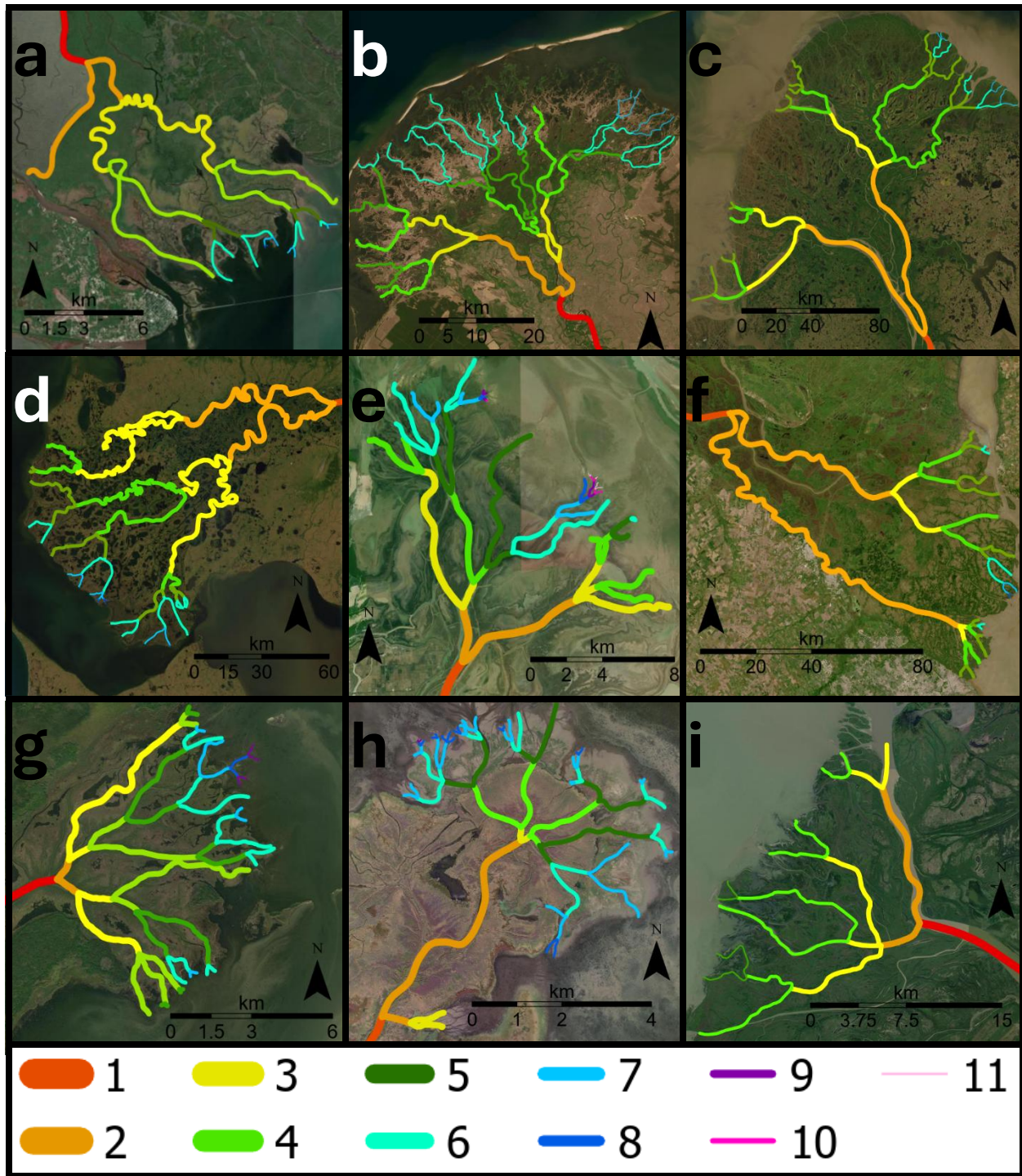


Figure 1: Examples of delta channel networks: (a) Apalachicola, (b) Selenga, (c) Yukon, (d) Kobuk, (e) Poyang Lake, (f) Parana (g) Saskatchewan, (h) Mamawi lake, (i) Slave deltas. The colors indicate channel hierarchy (see Methods). Base imagery from Esri's World Imagery basemap (© Esri, DigitalGlobe, GeoEye, i-cubed, USDA FSA, USGS, AEX, Getmapping, Aerogrid, IGN, IGP, swisstopo, and the GIS User Community). Colors and relative line thicknesses indicate channel hierarchy (see Methods), with the widest lines representing order 1 channels and progressively thinner lines representing higher channel orders.

198 2.2 Fluvial Fans

199 Fluvial fans are fan-shaped landforms that form by river avulsions or “channel jumps” across a low-
200 gradient floodplain (Chakraborty et al., 2010; Martin & Edmonds, 2023). In contrast to deltas where
201 mouth-bar-driven bifurcations and backwater-driven avulsions are strongly controlled by hydrodynamics
202 near a receiving basin of standing water (Brooke et al., 2022; Chatanantavet et al., 2012; Ganti et al.,
203 2014), *avulsions* that form fluvial fans are driven by a topographic slope break (Ganti et al., 2014; Martin
204 & Edmonds, 2023). Increased likelihood of avulsions at the fan apex is a consequence of the gradient
205 reduction that triggers in-channel sediment aggradation (Parker et al., 1998). These avulsions result from
206 high channel bed aggradation rates that are considerably higher than on the surrounding floodplains
207 (Pizzuto, 1987). Set up by in-channel aggradation, avulsions develop where a channel changes its course
208 due to channel superelevation (Bryant et al., 1995; Gearon et al., 2024; Mohrig et al., 2000) or a more
209 favorable (steeper) gradient at channel flanks (Gearon et al., 2024; Jones & Schumm, 1999; Slingerland &
210 Smith, 2004). Since the slope break controls the location of the fluvial fan’s apex, this avulsion node is
211 topographically pinned at this change in gradient, unlike in deltas (Ganti et al., 2014; Brooke et al., 2022).
212 Partial or full avulsions also occur further downfan, involving local gradient or discharge decreases, or
213 crevassing processes (Assine, 2005; Chakraborty et al., 2010; Donselaar et al., 2013; Gearon et al., 2024)
214 (Fig. 2).

215 Fluvial fan channel networks thus result through repeated nodal style avulsions (Slingerland & Smith,
216 2004) that typically shift the primary river to different regions of the fan (Chakraborty et al., 2010; Martin
217 & Edmonds, 2023; North & Warwick, 2007). These avulsions superimpose new channel positions on
218 paleo-channel locations and can split channels by partial avulsions and crevasses. This generates channel
219 and paleo-channel branching formed by processes distinct from deltas (North & Warwick, 2007) (Fig.
220 4b), where channel branching is predominantly caused by mouth-bar-driven bifurcations. In fluvial fans,
221 channel branching is related to avulsions, which generate channel networks that are predominantly paleo-
222 channel networks rather than active channel networks like in deltas (Chakraborty et al., 2010; North &
223 Warwick, 2007). Multiple channels can actively transmit discharge at partial avulsions, such as during
224 major river floods.

225 Downfan decreases in channel width have been well documented in modern and ancient fluvial fans
226 (Davidson et al., 2013; Kelly & Olsen, 1993; Nichols, 1987; Nichols & Fisher, 2007; Owen et al., 2015;
227 Wang & Plink-Björklund, 2019; Weissman et al., 2010), linked to discharge losses to floodplain
228 processes, infiltration into the loose sediments of the fan, and evapotranspiration (Davidson et al., 2013;
229 Hartley et al., 2010; Horton & Decelles, 2001; Weissman et al., 2010). However, some fluvial fan
230 channels have also been shown to widen downstream, possibly due to changes in channel planform or
231 aspect ratio, discharge contribution from groundwater, or discharge capture from adjacent rivers

232 (Chakraborty et al., 2010; Davidson et al., 2013). Fluvial fan channel networks have been studied for
233 qualitative descriptions of channel planform morphology (Davidson et al., 2013; Hartley et al., 2010;
234 Weissman et al., 2010) and scaling relationships (Davidson et al., 2013; Davidson & Hartley, 2014).
235 Modeling establishes a relationship between the fluvial fan shape and avulsion dynamics, like avulsion
236 trigger period and abandoned channel dynamics (Edmonds et al., 2022; Martin & Edmonds, 2023).

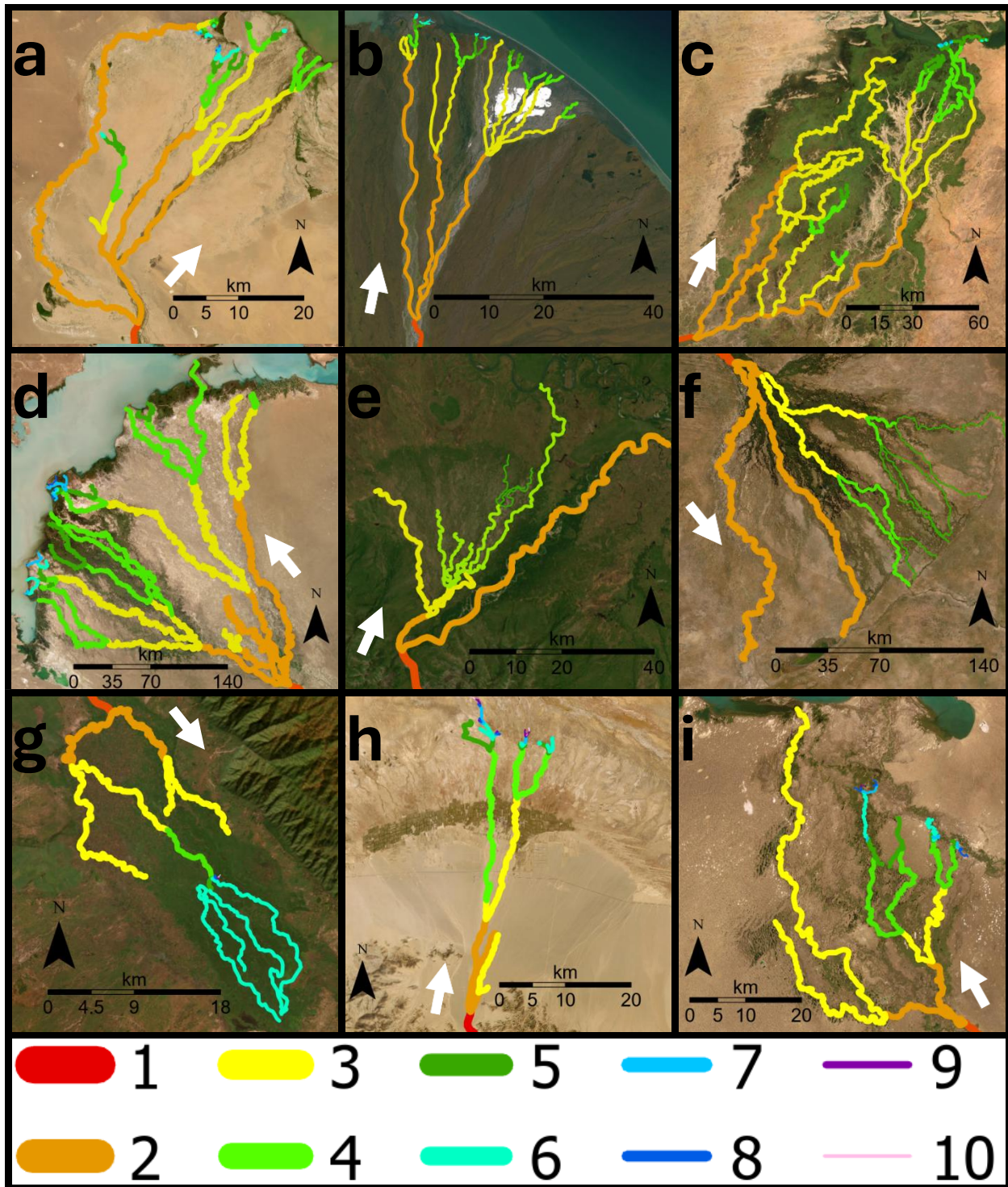


Figure 2: Examples of fluvial fan channel networks: (a) Dzavhan Gol, (b) Kongakut, (c) Niger, (d) Ili, (e) Bayunda, (f) Okavango, (g) Shire, (h) Nomon He, and (i) Aksu fans. The colors indicate channel hierarchy (see Methods), and white arrows indicates downfan direction. Base imagery from Esri's World Imagery basemap (© Esri, DigitalGlobe, GeoEye, i-cubed, USDA FSA, USGS, AEX, Getmapping, Aerogrid, IGN, IGP, swisstopo, and the GIS User Community). Colors and relative line thicknesses indicate channel hierarchy (see Methods), with the widest lines representing order 1 channels and progressively thinner lines representing higher channel orders.

238 Fluvial fans are distinct landforms from alluvial fans that feature steep gradients (typically 2–12°),
239 have a relatively small radial distance typically less than 10 kilometers, and lack channel networks (Blair
240 & McPherson, 1994; Moscariello, 2018). Although surface channels may occur on alluvial fans, these are
241 transient features formed by surface erosion, and do not construct alluvial fans, which form by a
242 combination of gravitational and sheet flood processes (Blair & McPherson, 1994; Moscariello, 2018).
243 Thus, alluvial fans are not considered here as they are distinct from fluvial fan channel networks that form
244 by river avulsions.

245 2.3 Morphometric Criteria for Recognition of Delta and Fluvial Fan Channel Networks

246 Based on the above differences in delta and fluvial fan morphodynamics, we hypothesize that the
247 morphometric differences in their channel networks can be quantified. Based on prior work, we expect
248 river-dominated delta channel networks to display downstream decreasing channel widths and lengths
249 with increasing bifurcation order (Edmonds & Slingerland, 2007; Seybold et al., 2007; Wolinsky et al.,
250 2010), and have an average channel network angle of approximately 72° (Coffey & Shaw, 2017). These
251 metrics should differ in fluvial fans, because the channel networks are built by river avulsions rather than
252 mouth-bar-driven bifurcations. However, delta networks also experience (lobe-scale) avulsions, and we
253 expect some overlap in the network angles. Below, we test these morphometric criteria on 40 river-
254 dominated delta and 40 fluvial fan channel networks (Fig. 3).

255 3. Dataset and Methods

256 Although automated channel mapping tools like ChannelExtractor in TopoToolbox (Schwanghart &
257 Kuhn, 2010) and Rivamap (Isikdogan et al., 2017) exist, these methods rely on either terrain-based flow

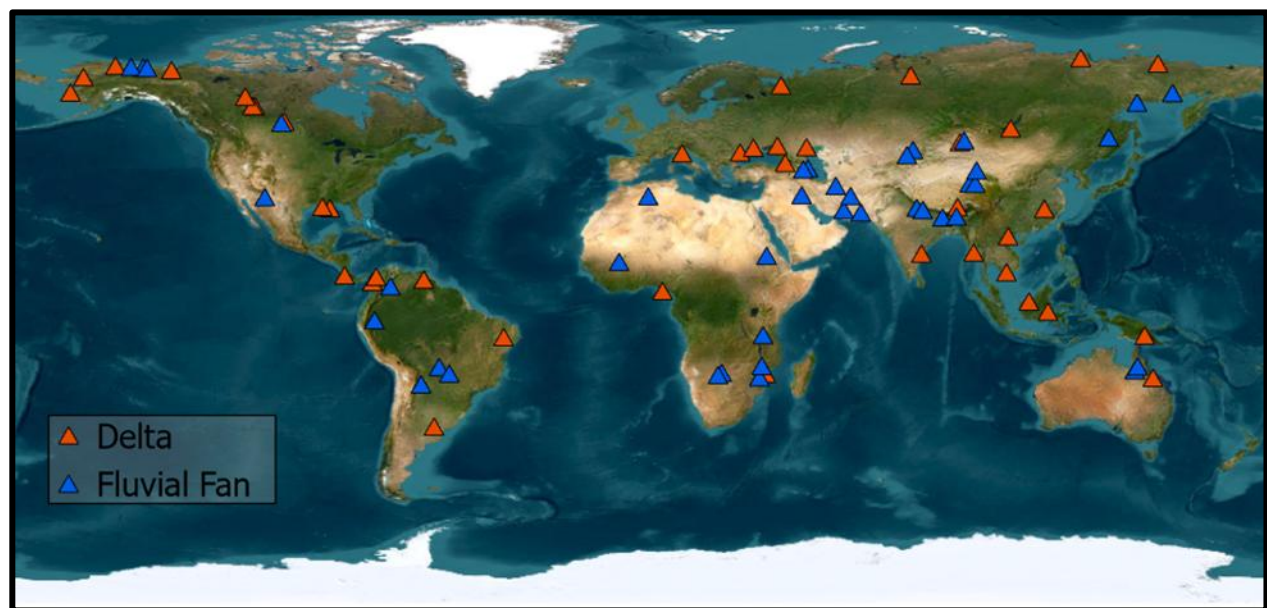


Figure 3: Map of deltas and fluvial fans in this study. Base imagery from Esri's World Imagery basemap (© Esri, DigitalGlobe, GeoEye, i-cubed, USDA FSA, USGS, AEX, Getmapping, Aerogrid, IGN, IGP, swisstopo, and the GIS User Community).

258 routing or the detection of active surface water, typically based on spectral characteristics, to delineate
259 river channels. However, fluvial fan channel networks are predominantly composed of paleo-channels
260 that lack both clear topographic expression and surface water signatures. Both delta and fluvial fan
261 channels can also be only a few meters wide, often falling below the spatial resolution of commonly
262 available DEMs and remote sensing imagery. In such settings, the coarse resolution and smoothing of
263 subtle terrain in DEMs, especially in low-relief environments, further limit the effectiveness of automated
264 extraction. As a result, we are constrained to manual digitization, as described below.

265 **3.1 Channel Order**

266 To establish channel order in networks, we follow (Dong et al., 2016). Their method follows a simple
267 rule: bifurcations produce downstream increasing channel order through channels that branch. To be
268 considered a channel of a higher order, the resultant channels must not merge downstream. When a first-
269 order channel bifurcates, two second-order channels develop downstream of this bifurcation. When these
270 two channels subsequently bifurcate, two new pairs of third-order channels form, and so on (Figs. 4a and
271 4b). All channels from the first instance of branching up to and include those that enter a body of water or
272 terminate on land are measured. Identification of bifurcation nodes follows Edmonds et al., (2011), such
273 that the first-order bifurcation for a river channel is the first bifurcation that the channel undergoes (Fig.
274 4a). Although these methods were developed for deltaic channel networks, here we adapt them for fluvial
275 fan networks also (Figs. 4c and 4d). We do not map or measure channels that loop or rejoin downstream,
276 or channels of non-fluvial origin, such as tidal channels or inlets (Smart, 1971; Tejedor et al., 2015) that
277 are not connected to the fluvial distributary channels. We also omit local avulsions on fluvial fans, which
278 generate channels that typically merge downfan (Slingerland & Smith, 2004). Paleo-channels on fluvial
279 fans were recorded where possible. Paleo-channels resembled active channels that exhibit little to no
280 discharge when we mapped the channel networks (Fig, 4d). We included paleo-channel measurements in
281 fluvial fans because they are ubiquitous in fluvial fans (Hartley et al., 2010), and many of these channels
282 do carry discharge if reactivated during major flood events.

283 **3.2 Channel Length and Width Measurements**

284 Channel length and width measurements follow Edmonds & Slingerland (2007), where channel
285 length is measured as the distance between two bifurcation nodes in deltas (Fig. 4a). We adopt this
286 methodology also to fluvial fans to measure channel lengths between avulsion nodes (Fig. 4c). The
287 average width of a channel segment is recorded from three separate width measurements: one
288 immediately after a node (w_i), one immediately before the next node (w_f), and one halfway between these
289 two points at the midpoint of the channel segment (w_h) (Figs. 4a and 4c). Land–water boundaries in both
290 deltas and fluvial fans were identified visually based on color (with water appearing darker and bluer than
291 land), surface texture, and vegetation contrast. In deltas, channel width measurements were recorded

292 based on the width of water present in the channel, which was nearly always delineated by clear
 293 vegetation (Fig. 4b). For channels on fluvial fans, including paleo-channels, bankfull widths were
 294 measured from clearly identifiable channel banks, vegetation patterns, and subtle depressions, allowing

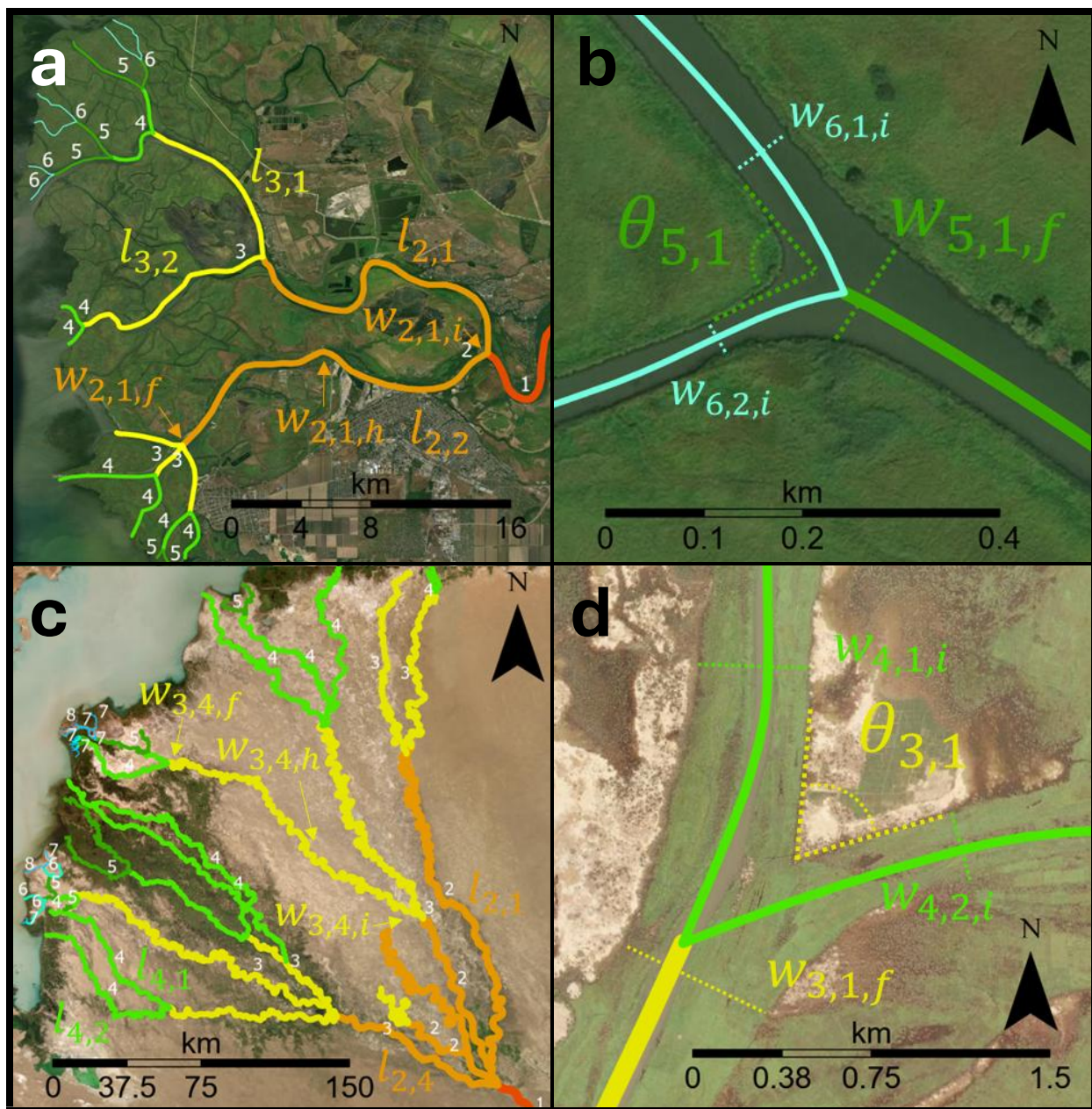


Figure 4: Illustration of (a) channel order, length, and width and (b) bifurcation angle measurements in deltas (Don delta). Illustration of (c) channel order, length, and width (Ili fan) and (d) divergence/crossover angle measurement (Niger fan). Arrows point to locations of w_i = initial channel width, w_h = midpoint channel width, w_f = final width measurements. The w_f is set as the length of two limbs that track along the edges of the mouth bar. θ_n corresponds to the bifurcation or divergence/crossover order. Base imagery from Esri's World Imagery basemap (© Esri, DigitalGlobe, GeoEye, i-cubed, USDA FSA, USGS, AEX, Getmapping, Aerogrid, IGN, IGP, swisstopo, and the GIS User Community).

295 for the mapping of dry or inactive channels (Fig. 4d). These approaches allowed measurement of inactive
296 channels while maintaining a uniform methodology and consistency for all width measurements. The
297 smallest measured channel widths resolvable in the imagery were 2-meters for deltas and 1-meters for
298 fluvial fans. Width measurements were not performed in locations where a channel has locally split into
299 multiple branches that join downstream.

300 Given the maximum 0.5-meter spatial resolution of the imagery (see Methods section 3.5), measuring
301 channels only a few meters wide carries some uncertainty. Normalization to the first-order channel width
302 helps mitigate this effect and reduce variability across systems. All channel width measurements were
303 normalized using the initial first-order channel width, following the methodology of Edmonds &
304 Slingerland, (2007). Consequently, the normalized channel width value for first-order channels is always
305 equal to one. First-order channel lengths were measured between the last occurrence of tributary channels
306 and the first channel splitting node and contain no significant value for our study. Moreover, manual
307 digitization of fluvial fan channels spanning tens of kilometers may introduce minor inconsistencies in
308 channel path representation, particularly for narrow (<10 m) and highly sinuous channels. All channel
309 length measurements (l) were also normalized using the first order channel width measurements
310 according to existing methodologies (Edmonds & Slingerland, 2007; Jerolmack, 2009), and this too
311 helped to reduce uncertainties when digitizing channel lengths. As such, the normalized first order
312 channel length values merely reflect our selected methodologies rather than an attributable morphological
313 characteristic.

314 **3.3 Network Angle Measurements**

315 To quantify network angles, we adopt the methodology of Coffey & Shaw, (2017) developed for
316 measuring channel bifurcation angles, which determines the angles of mouth bars formed at the end of an
317 upstream channel. In this methodology, the final channel width directly upstream of a bifurcation (w_f) is
318 set as the length for two limbs of an angle that follows the mouth bar-water contact to measure a
319 bifurcation angle (θ_n) (Coffey & Shaw, 2017) (Fig. 4b). The same methodology is adapted here for fluvial
320 fans (Fig. 4d). In some river deltas, tidal processes cause bifurcation of a channel into three channels
321 instead of two; these are referred to as trifurcations (Leonardi et al., 2013), furcation (Shaw et al., 2018)
322 or polyfurcations (Chamberlain et al., 2018), and a few such measurements are included in the dataset in
323 the very distal portions of deltas where tidal influence is significant. We do not measure angles where
324 channels loop or rejoin downstream of avulsions or bifurcations. In essence, we focus on the morphology
325 of branching channel networks and measure the visible angles between channels or paleo-channels
326 independent of their origin (Fig. 4b and 4d).

327 **3.4 Global Delta and Fluvial Fan Channel Network Database**

328 To test the applicability of the proposed criteria, we selected 40 river-dominated deltas and 40
329 fluvial fans (Fig. 3 and Supplementary Data) to be mapped using composite satellite data (ESRI, 2025).
330 These landforms were selected from a diverse range of hydroclimatic, topographic, and basinal conditions
331 from across the world (Fig. 3).

332 All deltas have been identified as such by prior work (Broaddus et al., 2022; Galloway, 1975;
333 Hartley et al., 2010; Leier et al., 2005; Nienhuis et al., 2015, 2018; Vulis et al., 2023), and they display
334 active discharge based on satellite imagery. Only river-dominated deltas are included in the dataset,
335 because wave- and tide-dominated delta morphology is distinct from that of fluvial fans. The river
336 dominance of deltas and the presence of tide- or wave-influence was determined using the established
337 principles of process-based delta classification (Broaddus et al., 2022; Galloway, 1975; Nienhuis et al.,
338 2015, 2018; Paniagua-Arroyave and Nienhuis 2024; Vulis et al., 2023). However, categorical
339 discrepancies exist between these different classification approaches. To clarify our terminology, we
340 define “dominated” versus “influenced” deltas as follows. Wave-dominated deltas (e.g. São Francisco,
341 Eel) are characterized by strandplanes and a complete absence of bifurcations; these deltas are excluded
342 from our study. Wave-influenced deltas still possess morphological features such as strandplains, but
343 exhibit clear, measurable channel bifurcations and are included in our study. Similarly, tide-dominated
344 deltas (e.g. Fly, Yangtze) have a limited number of channels that widen substantially seaward, whereas
345 tide-influenced deltas such as the Yukon (Fig. 1c) exhibit channel widening only in the most distal
346 channels (Xu & Plink-Björklund, 2023). In practice, we combine these parameters with established
347 classifications (Broaddus et al., 2022; Galloway, 1975; Nienhuis et al., 2015, 2018; Paniagua-Arroyave &
348 Nienhuis, 2024; Vulis et al., 2023) to categorize the deltas in our study. Please refer to the Supplementary
349 Data for information regarding our classification of each delta. We test the effects of tide- and wave-
350 influence on the morphometric criteria by comparative analyses.

351 Fluvial fans were located using their apex coordinates from the global fluvial fan database of
352 Hartley et al. (2010). This database also includes data on fluvial fan length, gradient, termination style
353 (axial, contributory, lacustrine, marine, playa, desert/dune, and wetland). Termination styles refer to the
354 environment where the fluvial fan terminates: for instance, a contributory-termination style denotes that
355 the landform channels switch from distributary to contributory at the toe of the fan, while axial fans are
356 classified when the main channel forms a confluence with an axial fluvial system (Hartley et al., 2010).
357 Fluvial fans that enter oceans or lakes were originally distinguished from deltas based on (1) displaying
358 no significant modification of the planform by marine processes, such as wave or tidal influence; or (2)
359 the fluvial fans apex is close to the tidal limit (Hartley et al., 2010). They identified that on relatively
360 high-gradient systems (with slopes above 0.143°) marine reworking is normally restricted to the toe of the
361 fluvial fans and can be easily identified. On relatively low-gradient systems (with slopes below 0.0573°)

362 the influence of marine processes was more difficult to determine, and unless the landform apex was
363 located a significant distance inland (>200 km) the landform was excluded from their database. We added
364 a visual inspection that the channel network is a paleo-channel network, and we test the robustness of the
365 classification by comparative analyses of fluvial fans with lake and ocean terminations vs terrestrial
366 terminations. To further test the robustness of our methodology, we analyze whether the landform size,
367 gradient, termination style, or wave- and tide-influence in deltas affect the results.

368 **3.5 Mapping with ArcGIS Pro**

369 Delta and fluvial fan channel networks were mapped using ArcGIS Pro software (Version 3.2.1)
370 (Fig. 1, 2, and 4) with the ESRI World Imagery basemap, which provides up to 0.5-meter imagery for
371 most of the world (ESRI, 2025). This resolution is suitable for mapping very narrow channels only
372 several meters wide. Alternative datasets such as Landsat (30-meter resolution) or Sentinel-2 (10-meter
373 resolution) are too coarse for this application; however they do contain multispectral bands that could be
374 very useful in defining land-water contacts in places where it is ambiguous for wider channels. While
375 ESRI World Imagery is compiled from multiple providers and acquisition times, producing mosaicked
376 tiles, we did not observe noticeable changes in channel appearance across tile boundaries (e.g., abrupt
377 changes in channel width or discharge).

378 Another limitation of our dataset is uncertainty regarding the timing of satellite image acquisition
379 relative to precipitation events. Precipitation increases discharge, thereby increasing measured channel
380 widths, particularly for fluvial fans in arid environments. Such events can also reactivate partial avulsions
381 and crevasses, which can potentially increase the apparent number of channels. However, none of the
382 selected systems exhibited observable seasonal or large-scale discharge changes across their channel
383 networks attributable to different timings in data collection. Additionally, because this study relies on
384 values normalized to the initial channel width, the effects of seasonal variability on channel width
385 measurements are minimized.

386 Two feature classes were created: one for deltas and one for fluvial fans. Each delta or fluvial fan
387 landform was then individually mapped as a shapefile layer under the corresponding feature class
388 (Supplementary Data). The shapefiles for channel networks were created as polyline features, which
389 allow users to manually trace individual river channel segments while automatically recording line
390 lengths. Channel widths and angles were measured using the line and angle measurement tools in ArcGIS
391 Pro. All data was recorded in the attribute table for each landform. This data was organized into Excel
392 documents and subsequently converted to Python- and Pandas- readable CSV files (Supplementary Data).

393 **3.6 Code and Statistics**

394 Kolmogorov-Smirnov and Shapiro-Wilk tests were first applied to determine whether the data are
395 normally distributed. Levene's test was used to test differences in variances of populations that do not

396 exhibit a normal distribution (Trauth, 2006). Independent samples or Welch's t-test were then applied to
397 test for a difference in means for populations with similar and dissimilar variances, respectively, while
398 one-sample t-tests were used to test comparisons of a subgroup against the overall population mean
399 (Trauth, 2006). For this study, a p-value less than 0.05 (5% significance level) suggests that the two
400 population distributions, variances, or means are not similar. Data confidence intervals were calculated
401 according to Mendenhall et al., (2012). Data analysis and visualization were performed using Python.
402 Open-source data visualization libraries Matplotlib (Hunter, 2007), NumPy (Harris et al., 2020), SciPy
403 (Virtanen et al., 2020), and Seaborn (Waskom, 2021) were utilized.

404 **4. Results**

405 **4.1 Delta and Fluvial Fan Channel Network Angles**

406 The mean channel network angle (θ_d) in deltas is 74.0° with a 95th percentile confidence interval of \pm
407 1.9° ($n = 527$) (Fig. 5a). The mean channel network angle (θ_f) in fluvial fans is $55.0^\circ \pm 2.0^\circ$ ($n = 520$)
408 (Fig. 5b). The delta and fluvial fan network angle populations are not normally distributed according to
409 both Kolmogorov-Smirnov (KS) and Shapiro-Wilk (SW) tests, with p-values less than 0.05. Levene's test
410 for statistical difference in variances also results in a p-value less than 0.05, suggesting population
411 variances are statistically different. A subsequent independent sample t-test suggests the means of delta
412 and fluvial fan angle populations are statistically different, with a p-value less than 0.05. All statistical
413 results are recorded in Supplementary Table 1 in the Supplementary Information.

414 We also reviewed the mean network angle of each individual delta and fluvial fan (θ_{Landform}) (Figs. 5c
415 and 5d), and these analyses reveal some overlap. All fluvial fans have mean angle values less than 60° ,
416 except for six landforms, or 15% of fluvial fans in this study. Four of these landforms have mean angles
417 larger than 60° (60.8° , 63.2° , 67.7° , 67.9°), and two larger than the delta mean of 73.7° (79.6° , 80.1°). All
418 individual deltas have mean network angles larger than 60° , except for one delta (59.3°). There are also
419 three deltas with mean angles around 60° (61.5° , 62.4° , 63.3°).

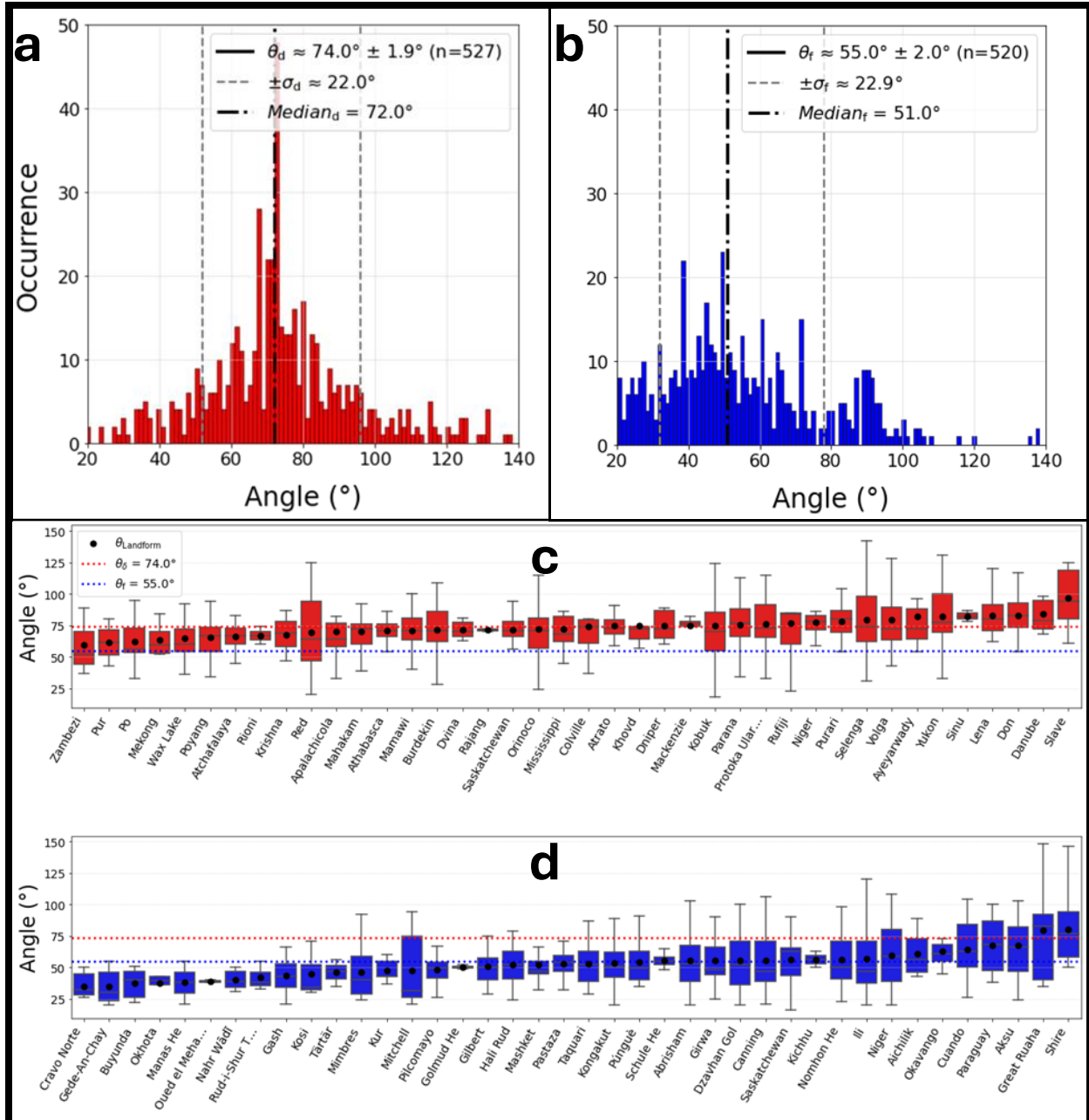


Figure 5: Histograms depicting distributions of (a) delta channel network angles with mean angle (θ_d), its standard deviation (σ_d) and median, and (b) fluvial fan channel network angles with mean fan angle (θ_f), its standard deviation (σ_f) and median. Box-and-whisker plots with the mean angle for each delta (c) and fluvial fan (d) landform ($\theta_{Landform}$).

420 The distribution of delta angles grouped by order (Fig. 6a) yields no strong trends for mean angle in
 421 deltas. Seventh and tenth order channels have slightly lower mean angle values at 65° and 67° , but these
 422 higher-order groups have low sample sizes ($n = 3$; $n = 8$) (Fig. 6a). The distribution of fluvial fan angles
 423 grouped by order does yield a trend: the mean angle for first- through third-order channels (θ_1 , θ_2 , and θ_3
 424 in Fig. 6b) is between $47 - 50^\circ$ and increases to $61 - 63^\circ$ for fourth- through eight-order channels, and to

425 66° for ninth-order angles ($n = 6$) ($\theta_4 - \theta_9$ in Fig. 6b). In contrast to the unimodal distribution of delta
 426 angles, the distribution of higher-order fluvial fan angles is bimodal, with a dominant peak near 50° and a
 427 secondary peak around 80 – 100° (Fig. 6b).

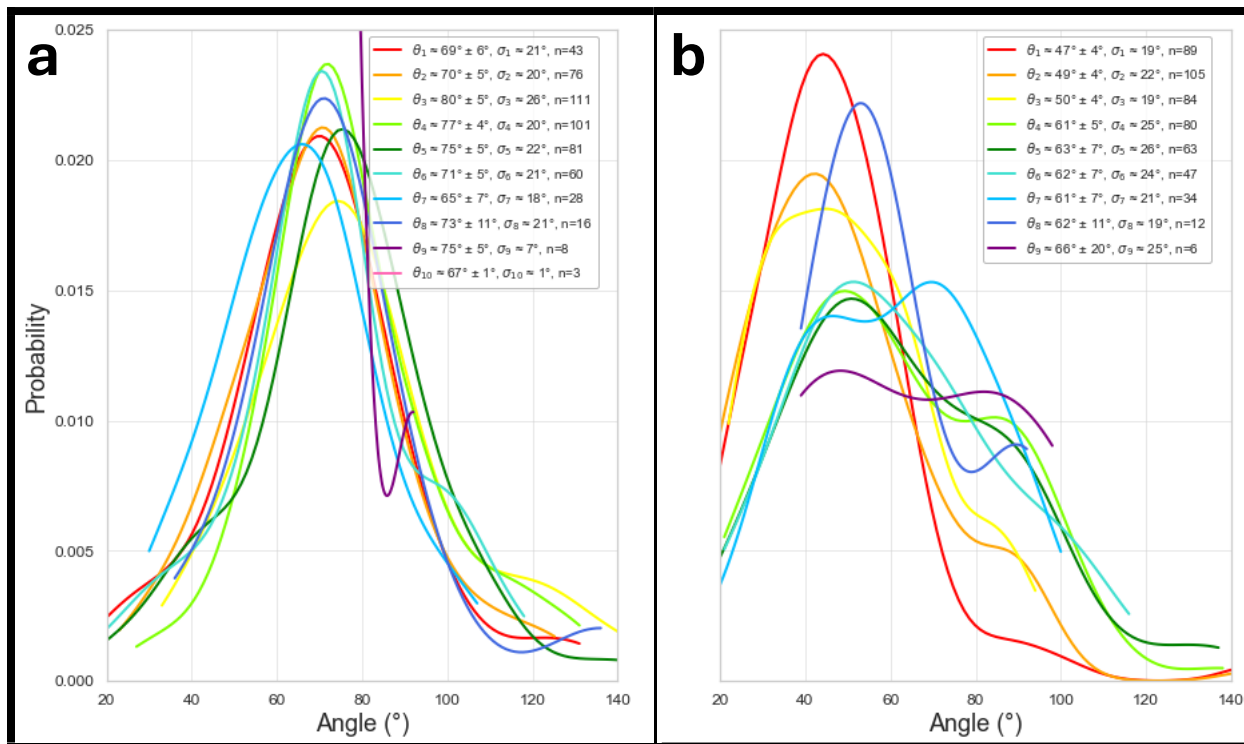


Figure 6: Distribution of (a) delta, and (b) fluvial fan network angles grouped by order (θ_n) with the 95th percent confidence interval. (σ_n) = denotes standard deviation. n denotes sample size.

428 All deltas in this analysis are river-dominated deltas, however some are tide- or wave-influenced (See
 429 Section 3.4 and Supplementary Data). Grouping deltas by process regime shows that the mean network
 430 angle for the 19 river-dominated deltas ($\theta_R = 73.6^\circ \pm 2.2^\circ$, $n = 374$), for the 16 tide-influenced deltas ($\theta_t =$
 431 $75.6^\circ \pm 3.9^\circ$, $n = 139$), and for the 5 wave-influenced deltas ($\theta_w = 67.1^\circ \pm 10.1^\circ$, $n = 14$) (Fig. 7a). The
 432 river-dominated and tide-influenced delta angle means are not statistically different from the mean angle
 433 for the whole delta population (Supplementary Table 1). The wave-influenced delta angles were omitted
 434 from this statistical analysis due to a small sample size ($n = 14 < 30$).

435 Many delta angle measurements in this dataset come from Arctic deltas. The comparison between
 436 Arctic and non-Arctic deltas shows that Arctic deltas have a larger mean angle ($\theta_A = 76.5^\circ \pm 2.7^\circ$, $n =$
 437 263) than non-Arctic deltas ($\theta_{NA} = 71.4^\circ \pm 2.6^\circ$, $n = 264$) (Fig. 7b). There is a statistically significant
 438 difference in means between Arctic and non-Arctic deltas (Supplementary Table 1). Grouping deltas by
 439 termination style (Fig. 7c) shows that lake-terminating deltas have slightly smaller mean angles than those
 440 that terminate in oceans ($\theta_L = 72.9^\circ \pm 3.2^\circ$, $n = 160$ versus $\theta_O = 74.4^\circ \pm 2.3^\circ$, $n = 367$), but these

441 differences are not statistically significant compared to the whole delta population (Supplementary Table
 442 1).

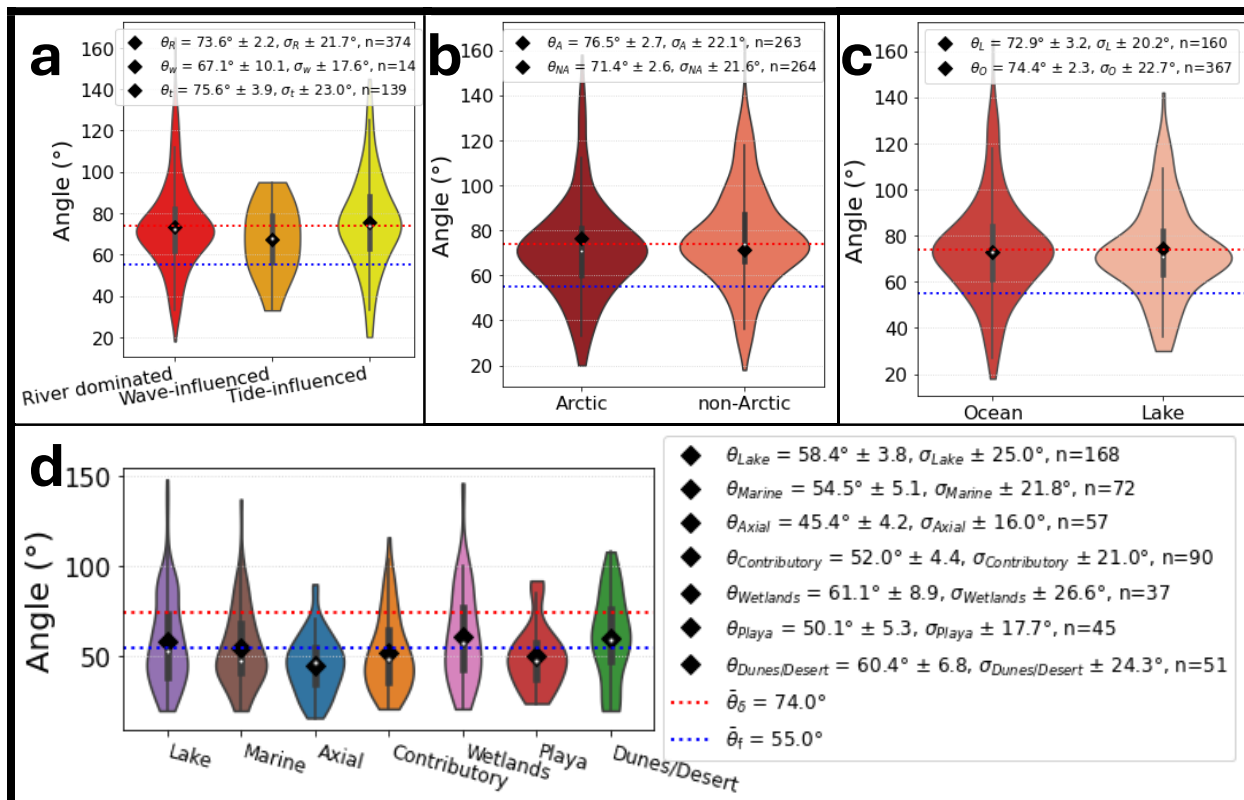


Figure 7: Violin plots depicting network angle distributions by (a) delta process regime: river dominated (θ_R), wave-influenced (θ_W), and tide-influenced (θ_T), (b) deltas in non-Arctic (θ_{NA}) and Arctic (θ_A) climates, (c) ocean terminating deltas (θ_O) and lake terminating deltas (θ_L), and (d) fluvial fan termination styles. All mean angle values have a corresponding 95th percent confidence interval, standard deviation (σ), and sample count (n).

443 Grouping fluvial fans by their termination style shows some differences (Fig. 7d), where the mean
 444 angles vary from a low of $\theta_{Axial} = 45.4^\circ \pm 4.2^\circ$ ($n = 57$) for axial-terminating fluvial fans to $\theta_{wetlands} = 61.1^\circ$
 445 $\pm 8.9^\circ$ ($n = 37$) for wetland-terminating fans (Fig. 7d). All fluvial fan termination types, except for axial-
 446 terminating fans, exhibit population means that are statistically similar to the overall fluvial fan
 447 population (Supplementary Table 1). However, each termination style is represented by only 4 to 6
 448 landforms, limiting the statistical power of comparisons and generalizations, despite the relatively robust
 449 measurement numbers in wetland ($n = 37$), playa ($n = 45$), dunes/desert ($n = 51$), and axial-terminating
 450 fans ($n = 57$). There also appears to be some discrepancies in Hartley et al., (2010)'s assignment of
 451 termination types, such as referring to playa fans as lacustrine or ocean fans as contributory. We also
 452 tested whether landform size (Supplementary Fig. 1) and gradient (Supplementary Fig. 2) affect the
 453 channel network angles, and these analyses yield no trends, supporting the robustness of our
 454 methodology.

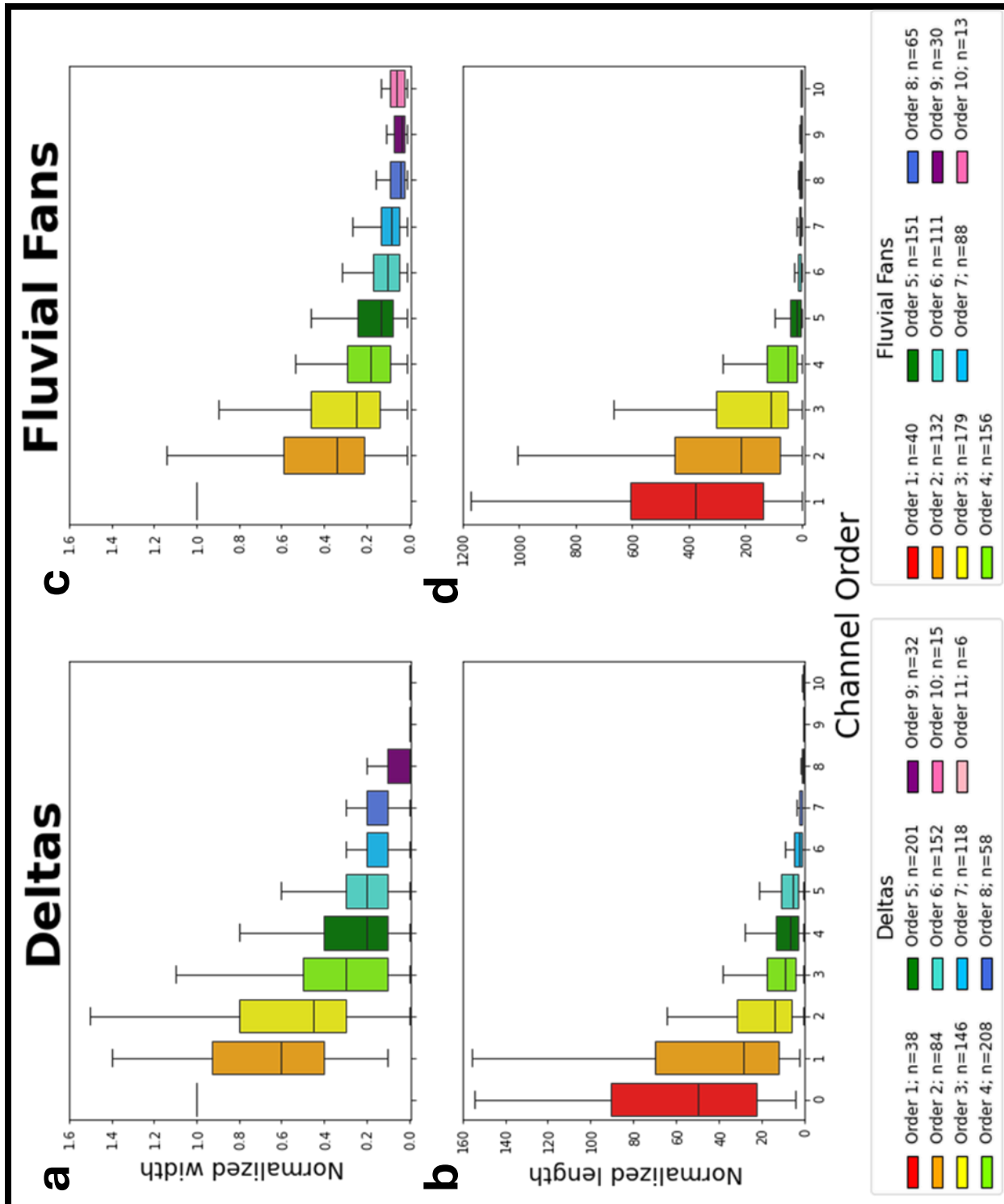
455
456
457
458
459
460
461
462
463
464
465
466
467
468
469
470
471
472
473
474
475
476
477
478
479
480
481
482
483
484
485

4.2 Channel Lengths and Widths

Normalized channel length and width measurements reveal morphological differences between fluvial fan and delta channels. Both landform types show non-linear decreases in these values with increasing channel order (Fig. 8). Statistical analyses confirm that the overall means for normalized channel length and width differ significantly between fluvial fans and deltas (Supplementary Table 1). Fluvial fan channels are generally an order of magnitude longer than delta channels, with a mean normalized length of 147.09 compared to 17.18 for deltas (Figs. 8a and 8c). In contrast, delta channels tend to be slightly wider, with a mean normalized width of 0.40 compared to 0.26 for fluvial fans (Figs. 8b and 8d).

Comparing the normalized dimensions by channel order (Fig. 9) reveals additional trends. The normalized channel widths of lower-order fluvial fan channels (orders 1–5) are significantly longer, and the channel shortening rate is higher compared to deltas (Fig. 9a). The normalized lengths become very similar in orders 7–8, then diverge again for the higher orders where the fluvial fan channel lengths are somewhat longer, but the channel shortening rates are higher in deltas. Normalized channel widths show significant differences for orders 2–8, but not for 9–11. Only a few landforms have channels with orders exceeding 9. Fluvial fan narrowing rates are very high from order 1 and 2, and very low in orders 7–10 (Fig. 9b). The narrowing rates are more uniform in deltas. When comparing individual deltas by process regime, both tide- and wave-influenced deltas have significantly higher mean normalized channel widths relative to the overall delta population (Supplementary Fig. 3 and Supplementary Table 1).

Comparison by fluvial fan termination styles shows that axial- and playa-terminating fans exhibit longer mean normalized channel lengths compared to the whole fluvial fan population, whereas dunes/desert-, marine-, and wetland-terminating fans have shorter mean lengths (Supplementary Fig. 3 and Supplementary Table 1). Contributory- and lake-terminating fans do not differ significantly from the overall mean. Regarding normalized channel widths, axial- and marine-terminating fans have wider channels, while dunes/desert-terminating fans are narrower. Normalized width values for contributory-, lake-, playa-, and wetland-terminating fan channels show no difference from the overall population mean (Supplementary Fig. 3 and Supplementary Table 1). Statistical analyses of channel length and width were not conducted for different fluvial fan termination styles due to insufficient sample sizes ($n < 30$) in most categories.



486 Figure 8: Box and whisker plots illustrating normalized delta channel widths (a) and lengths (b), and normalized fluvial fan channel widths (c) and length (d), plotted by channel order. Note the significant difference in normalized channel length scales for subplots b and d.

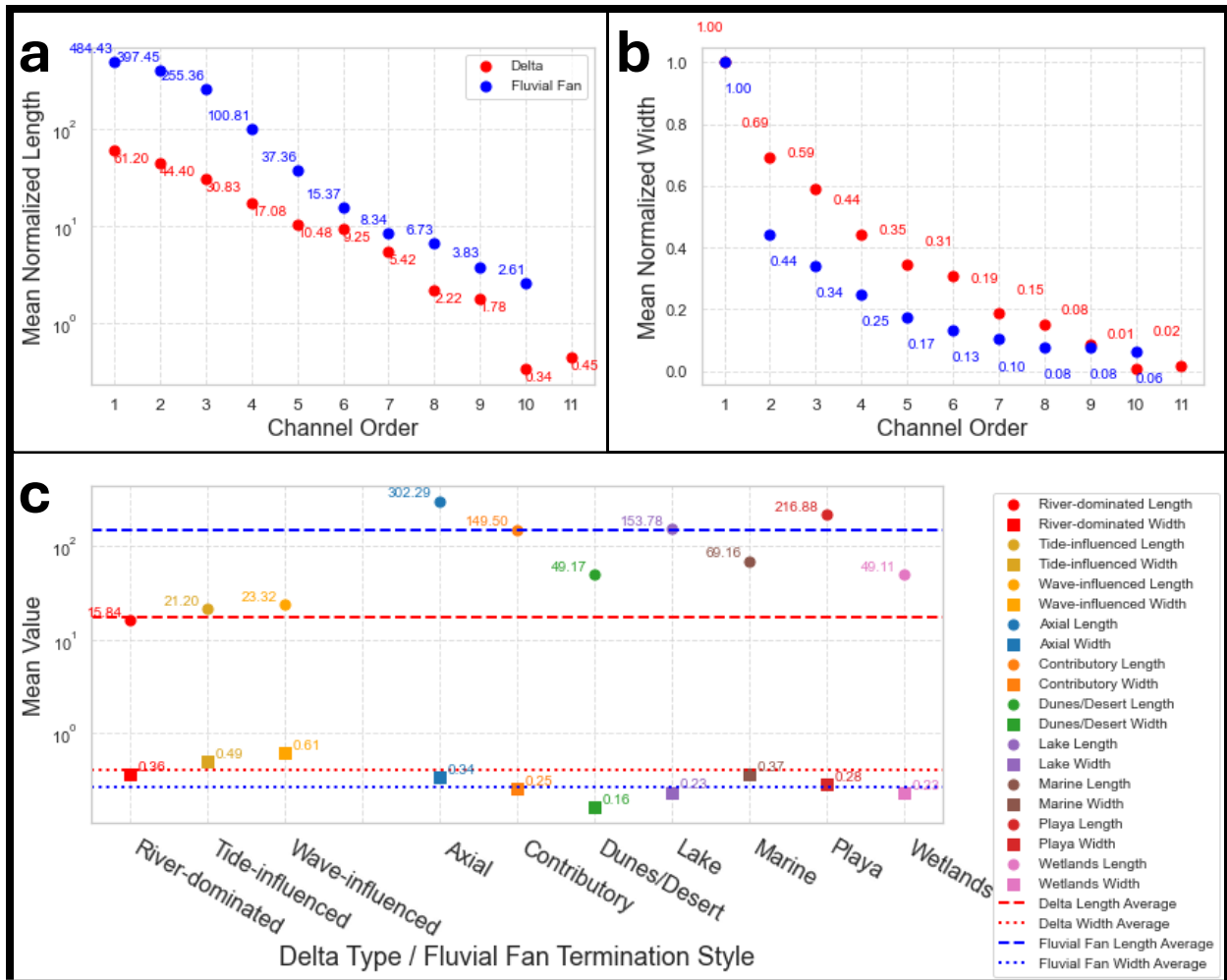


Figure 9: Mean normalized delta and fluvial fan channel (a) length and (b) width values by order. (c) Mean channel length and width values for different types of deltas and fluvial fan termination styles.

487

488 **5. Discussion**

489 **5.1 Effectiveness of Morphometric Criteria in Distinguishing Deltas and Fluvial Fans**

490 The mean channel network angles are distinctly different in deltas and fluvial fans by 20°, and this
 491 statistically significant difference is a useful criterion in distinguishing these two landform types. While
 492 some overlaps exist at the landform level, these cases are relatively limited, where 15% of fluvial fans in
 493 this dataset have a mean angle larger than 60° (Fig. 5d) and 10% of deltas have a mean angle less than
 494 64° (Fig. 5c). These findings support the utility of mean branching angles as a distinguishing metric
 495 between deltas and fluvial fans. However, some degree of uncertainty remains, and additional criteria are
 496 necessary for more robust distinction.

497 An additional criterion is the distribution of mean angles by channel order, where fluvial fans have
 498 increased mean angles and a bimodal distribution in orders 4–8 (Fig. 6). Other supportive criteria may be
 499 the differences in values and distributions of the normalized channel lengths and widths (Figs. 8 and 9),

500 but the low sample numbers do not allow us to test these criteria by individual landforms. A useful
501 criterion would be to link channel narrowing with the bifurcation and avulsion nodes. In deltas, the
502 downstream channel narrowing occurs in a stepwise manner at the mouth-bar-driven bifurcation nodes,
503 whereas in fluvial fans this decrease should be gradual and not linked to the node positions where full
504 avulsions occur. Our data was collected in a manner that does not permit these analyses.

505 A potential source of overlap in the delta and fluvial fan channel network mean angles is that not all
506 measured angles in deltas are mouth-bar-driven bifurcation angles, as deltas also experience avulsions
507 (e.g., Fig. 1e). A closer inspection of the four deltas with low mean network angles reveals that each
508 contains very few measurements ($n = 3$, $n = 4$, $n = 6$, $n = 7$). In these cases, the limited sample size allows
509 the rarer avulsion angles to affect the mean values more strongly. Also, fluvial fans that terminate in a
510 lake or ocean may have terminal channels that form due to mouth bar deposition and channel bifurcation.
511 However, we do not believe these instances affect our results since we do not see that lake- or marine-
512 terminating fans exhibit higher mean angles (Fig. 7d).

513 Examining fluvial fans with high mean angles shows that these are low-gradient wetland fans, where
514 the avulsion angles tend to be wider as a function of avulsion mechanisms (see Discussion below).
515 However, they may also suggest methodological limitations. While the local avulsion angles in low-
516 gradient wetland fans are wide (measured the final channel width directly upstream of a branching node
517 (w_f) as the length for two limbs of an angle; Fig. 4), angles between the longer channel reaches are
518 considerably narrower (Supplementary Fig. 4). This channel reach angle discrepancy is consistent with
519 similar channel reach angle measurements from (Coffey & Shaw, 2017). We plan to further develop angle
520 measurement methods to capture both the local and the reach-scale angles in future work. It is also
521 important to discuss the limitations of the applied methodologies in the context of the results. Our channel
522 network methodologies are designed for delta channel networks, and exclude channels that merge
523 downstream, which can exclude many potential measurements from fluvial fans in situations where their
524 channels merge downfan.

525 In summary, this initial attempt to distinguish deltas and fluvial fans demonstrates that quantifying
526 channel network angles, and trends in normalized channel widths and lengths provide efficient criteria.
527 However, we also show that sample sizes are important for accurate recognition of landforms, and
528 collecting a sufficient number of angle measurements ($n \gtrsim 10$) can help account for the infrequent
529 avulsion in deltas or bifurcation in fluvial fans. While each metric is informative on its own, the
530 combination of branching angles, branching angle trends, and normalized channel lengths provides the
531 clearest distinction between deltas and fluvial fans.

532 **5.2 Processes that determine delta and fluvial fan channel network angles**

533

534 While the 72° mean mouth-bar-driven bifurcation angle is linked to flow patterns at channel tips well-
535 explained by diffusive processes (Coffey & Shaw, 2017), there is currently no established explanation for
536 the approximately 55° mean network angle in fluvial fans. In deltas, mouth-bar-driven bifurcation is the
537 product of sedimentation from turbulent jets that form at the mouths of rivers entering basins (Bates,
538 1953; Coffey & Shaw, 2017; Edmonds & Slingerland, 2007; Fagherazzi et al., 2015; Jerolmack &
539 Swenson, 2007; Wright, 1977). Once a mouth bar is formed, the flow through the distributary channel
540 bifurcations can be modeled as diffusive flow (Coffey & Shaw, 2017), and the resulting critical angle of
541 72° represents a stable morphology for the bifurcation as it grows in a diffusive groundwater field
542 (Devauchelle et al., 2012; Ke et al., 2019). The slightly larger network angles in Arctic deltas may reflect
543 environmental influences such as ice cover, permafrost, or limitations on overbank flow (Lauzon et al.,
544 2019; Piliouras et al., 2021; Walker, 1998).

545 River avulsions are set up by channel superelevation (Mohrig et al., 2000), or when the slope down
546 the flanks of the channel provides a steeper descent than the existing river channel (Slingerland & Smith,
547 1998; Törnqvist & Bridge, 2002). Avulsions result from channel bed aggradation that reduces the channel
548 capacity (Bryant et al., 1995). Once an avulsion is triggered and full or partial river flow exits the channel,
549 a new channel is generated by surface runoff erosion. Thus, the prevailing topographic gradient would
550 tend to keep the nearby flows more focused in a slope-parallel direction, resulting in narrower network
551 angles compared to mouth-bar-driven bifurcations (Fig. 5b).

552 The contrast between diffusion-dominated and surface runoff erosion-dominated processes in shaping
553 delta versus fluvial fan channel network topology is further supported by tributary channel network
554 analyses that originally defined the critical angle of 72° (Devauchelle et al., 2012). Tributary channel
555 network analyses show that the mean tributary angle of 72° only occurs in humid catchments with high
556 groundwater recharge, where tributary networks are shaped by groundwater diffusion (Seybold et al.,
557 2017). In contrast, the mean tributary network angle is 45° in arid landscapes where surface runoff
558 dominates (Seybold et al., 2017), or is even lower in the driest catchments (Seybold et al., 2018).

559 Fluvial fan gradient decreases progressively downstream (e.g. Chakraborty et al., 2010), such that
560 higher gradients near the fan apex likely generate more acute angles, whereas the very low gradients near
561 the toe of the fan would allow for wider angles. This trend likely explains the downstream increase in
562 fluvial fan network angles and the emergence of the second, wider peak in higher order channels (Fig.
563 6b). Furthermore, avulsion mechanisms have been shown to change from channel superelevation in
564 upstream river reaches, where river gradients are steeper, to gradient advantage in downstream low-
565 gradient reaches (Gearon et al., 2024). In these low-gradient zones, crevassing processes can produce
566 high-angle deviations with the angle values around 90° (Rahman et al., 2022). Avulsion angles above
567 100° have been measured in meandering rivers on low-gradient floodplains with vegetation (see Rahman

568 et al., 2022). These effects may be important controls in the fluvial fan channel networks in low-gradient
569 vegetated wetlands. Reitz & Jerolmack, (2012) show that abandoned paleo-channel reoccupation may
570 control new avulsion positions, and paleo-channel density is highest in the narrower fan apex. Avulsion
571 angles may also change over time due to evolving channel width ratios (Morais & Montanher, 2022), or
572 may be affected by a critical angle or bend curvature (Yang, 2020). Future work targeting how avulsion
573 morphology evolves downfan would provide important insight into the mechanisms driving the observed
574 increase in angles downstream.

575 We thus conclude that the distinction between deltaic and fluvial fan channel network angles arises
576 from the dominant formative processes: diffusive flow in deltas versus surface runoff erosion in fluvial
577 fans. Furthermore, in fluvial fans, network angles appear to be negatively correlated with surface
578 gradients, with lower gradients allowing for wider avulsion angles.

579 **5.3 Ancient deltas and fluvial fans**

580 Our proposed methodology could also be used to distinguish ancient fluvial fans and deltas, for
581 instance in seismic datasets, where only delta channel network angles have been quantified before
582 (Mahon et al., 2024). Our results confirm the prior modern data (Chakraborty et al., 2010) and recent
583 modeling outcomes (Martin & Edmonds, 2023), and help to eliminate a discrepancy in plan-view versus
584 cross-sectional fluvial fan facies models (Plink-Björklund, 2021). Namely, earlier work suggested
585 processes similar to mouth-bar-driven bifurcations as a key mechanism driving fluvial fan formation
586 (Friend, 1978; Kelly & Olsen, 1993; Weissman et al., 2010), probably due to downstream channel
587 narrowing. However, this hypothesis contradicts the stratigraphic data that indicate that proximal fans
588 consist of amalgamated channel deposits (Chakraborty et al., 2010; Kelly & Olsen, 1993; Nichols &
589 Fisher, 2007; Singh et al., 1993; Weissman et al., 2013) – a pattern consistent with frequent avulsions
590 (Chakraborty et al., 2010; Singh et al., 1993).

591 **5.4 Sensitivity of Deltas and Fluvial Fans to Global Change**

592 Deltas and fluvial fans differ significantly in their vulnerability to natural hazards and in their
593 responses to global change. Deltas are highly vulnerable to coastal hazards and sea level rise (Giosan et
594 al., 2014; Syvitski et al., 2009). Rising sea-levels will not only inundate deltaic distributary networks, but
595 also cause a landward migration of the avulsion node corresponding with the landward shift of the
596 backwater zone (Brooke et al., 2022; Chatanantavet et al., 2012; Ganti et al., 2014). This process reduces
597 sediment delivery to shorelines, accelerating the effects of sea-level rise. However, changes in land use
598 and changing precipitation patterns which increase sediment supply could complicate the picture by
599 shifting delta avulsion sites seaward (Brooke et al., 2022). In contrast, fluvial fans are controlled by
600 upstream morphodynamics, where the fan location (apex) is pinned by a steep topographic break (Brooke
601 et al., 2022; Ganti et al., 2014; Martin & Edmonds, 2023). For coastal fans, sea-level rise and coastal

602 erosion would affect the fan toes, however the avulsion node at the fan apex and sediment deposition
603 across most of the fan surface would not be affected, making fluvial fans significantly less vulnerable to
604 sea-level rise.

605 Both deltas and fluvial fans are affected by reduced sediment supply due to river damming and
606 artificial levees (Blum & Roberts, 2009; Giosan et al., 2014; Nienhuis et al., 2020; Paola et al., 2011;
607 Syvitski et al., 2009). However, fluvial fans are highly sensitive to the water and sediment supply
608 changes, such as changes in precipitation patterns (Assine et al., 2014; Hansford & Plink-Björklund,
609 2020; Leier et al., 2005). Increases in extreme precipitation cause a significant increase in avulsion
610 frequency and crevassing splay formation (Morón et al., 2017), because large fluctuations in river
611 discharge, such as during extreme precipitation events, are avulsion-triggering events (Jones & Schumm,
612 1999). Indeed, fluvial fans have been shown to be highly sensitive to such changes, where fluvial fan
613 activation and deactivation cycles have been linked to millennial-scale changes in monsoon intensity or
614 precipitation patterns (Assine et al., 2014; Fontana et al., 2014, Latrubesse et al., 2012).

615 **6. Conclusions**

616 This study demonstrates that river-dominated delta and fluvial fan channel networks can be
617 distinguished using quantitative morphometric criteria derived from their channel network topology.
618 Deltaic networks are primarily shaped by mouth-bar-driven bifurcation processes, resulting in mean
619 bifurcation angles of approximately 74° , consistent with diffusion-dominated growth. In contrast, fluvial
620 fan topology is shaped by channel avulsions, producing narrower mean network angles near 55° ,
621 indicative of surface runoff processes. Fluvial fan network angles tend to widen downstream, likely due to
622 decreasing gradients and avulsion style shifts, while delta angles remain relatively consistent, reflecting
623 persistent mouth-bar-driven bifurcation processes. Both channel networks display downstream reductions
624 in channel length and width with increasing channel order, but the fluvial fan networks are characterized
625 by significantly longer and somewhat narrower channels when normalized.

626 These differences not only support the use of network morphology as a diagnostic tool for identifying
627 ancient fluvial fans and deltas in the stratigraphic record or other planetary bodies but also provide
628 insights into their differing sensitivities to environmental change.

629

630 **Code Availability**

631 The Python code used for data analysis and figure generation was created and run in Jupyter Notebook
632 version 6.4.8 (Anaconda distribution).

633

634 **Data Availability**

635 Morphological data collected in this study are available at [https://github.com/lukegezovich/Delta-and-](https://github.com/lukegezovich/Delta-and-Fluvial-Fan-Networks)
636 [Fluvial-Fan-Networks](https://github.com/lukegezovich/Delta-and-Fluvial-Fan-Networks).

637

638 **Author Contribution**

639 Luke Gezovich was responsible for the investigation and data curation, development of methodology,
640 formal analysis and visualization, and writing the original draft of the manuscript. Piret Plink-Björklund
641 initiated the project, co-developed the initial methodology, and co-wrote the manuscript. Jack Henry co-
642 developed the initial methodology and perform initial mapping and analyses of a small number of
643 systems.

644

645 **Competing Interests**

646 The authors declare that they have no conflict of interest.

647

648 **Acknowledgments**

649 We thank Kamini Singha, Lesli Wood, and Wendy Zhou for their constructive feedback that helped
650 improve earlier versions of this manuscript. We also thank John Shaw, Ellen Chamberlin, Anastasia
651 Piliouras, and an anonymous reviewer for their helpful comments on the present versions of the
652 manuscript.

653

654 **Financial Support**

655 Luke Gezovich thanks the American Association of Petroleum Geologists (AAPG) Foundation John &
656 Erika Lockridge Grant, the American Institute of Professional Geologists (AIPG) William J. Siok Graduate
657 Scholarship, the Colorado Scientific Society (CSS), the Rocky Mountain Association of Geologists
658 (RMAG), and the Society for Sediment Geology (SEPM) for providing funding to support this research.

659

660 **References**

661 Allen, P. A. (2008). Time scales of tectonic landscapes and their sediment routing systems. *Geological*
662 *Society, London, Special Publications*, 296(1), 7–28. <https://doi.org/10.1144/SP296.2>

663 Assine, M. L. (2005). River avulsions on the Taquari megafan, Pantanal wetland, Brazil. *Geomorphology*,
664 70(3–4), 357–371. <https://doi.org/10.1016/j.geomorph.2005.02.013>

665 Assine, M. L., Corradini, F. A., Pupim, F. D. N., & McGlue, M. M. (2014). Channel arrangements and
666 depositional styles in the São Lourenço fluvial megafan, Brazilian Pantanal wetland. *Sedimentary*
667 *Geology*, 301, 172–184. <https://doi.org/10.1016/j.sedgeo.2013.11.007>

668 Axelsson, V. (1967). The Laitaure Delta: A Study of Deltaic Morphology and Processes. *Geografiska*
669 *Annaler. Series A, Physical Geography*, 49(1), 1. <https://doi.org/10.2307/520865>

670 Bates, C. C. (1953). Rational Theory of Delta Formation. *AAPG Bulletin*, 37.
671 <https://doi.org/10.1306/5CEADD76-16BB-11D7-8645000102C1865D>

672 Bentley, S. J., Blum, M. D., Maloney, J., Pond, L., & Paulsell, R. (2016). The Mississippi River source-to-
673 sink system: Perspectives on tectonic, climatic, and anthropogenic influences, Miocene to
674 Anthropocene. *Earth-Science Reviews*, 153, 139–174. <https://doi.org/10.1016/j.earscirev.2015.11.001>

675 Blair, T. C., & McPherson, J. G. (1994). Alluvial Fans and their Natural Distinction from Rivers Based on
676 Morphology, Hydraulic Processes, Sedimentary Processes, and Facies Assemblages. *SEPM Journal of*
677 *Sedimentary Research*, Vol. 64A. <https://doi.org/10.1306/D4267DDE-2B26-11D7-8648000102C1865D>

678 Blum, M. D., & Roberts, H. H. (2009). Drowning of the Mississippi Delta due to insufficient sediment
679 supply and global sea-level rise. *Nature Geoscience*, 2(7), 488–491. <https://doi.org/10.1038/ngeo553>

680 Bramble, M. S., Goudge, T. A., Milliken, R. E., & Mustard, J. F. (2019). Testing the deltaic origin of fan
681 deposits at Bradbury Crater, Mars. *Icarus*, 319, 363–366. <https://doi.org/10.1016/j.icarus.2018.09.024>

682 Broaddus, C. M., Vulis, L. M., Nienhuis, J. H., Tejedor, A., Brown, J., Foufoula-Georgiou, E., & Edmonds, D.
683 A. (2022). First-Order River Delta Morphology Is Explained by the Sediment Flux Balance From Rivers,
684 Waves, and Tides. *Geophysical Research Letters*, 49(22). <https://doi.org/10.1029/2022GL100355>

685 Brooke, S., Chadwick, A. J., Silvestre, J., Lamb, M. P., Edmonds, D. A., & Ganti, V. (2022). Where rivers
686 jump course. *Science*, 376(6596), 987–990. <https://doi.org/10.1126/science.abm1215>

687 Bryant, M., Falk, P., & Paola, C. (1995). Experimental study of avulsion frequency and rate of deposition.
688 *Geology*, 23(4), 365. [https://doi.org/10.1130/0091-7613\(1995\)023%253C0365:ESOFA%253E2.3.CO;2](https://doi.org/10.1130/0091-7613(1995)023%253C0365:ESOFA%253E2.3.CO;2)

689 Chakraborty, T., Kar, R., Ghosh, P., & Basu, S. (2010). Kosi megafan: Historical records, geomorphology
690 and the recent avulsion of the Kosi River. *Quaternary International*, 227(2), 143–160.
691 <https://doi.org/10.1016/j.quaint.2009.12.002>

692 Chamberlain, E. L., Törnqvist, T. E., Shen, Z., Mauz, B., & Wallinga, J. (2018). Anatomy of Mississippi Delta
693 growth and its implications for coastal restoration. *Science Advances*, 4(4), eaar4740.
694 <https://doi.org/10.1126/sciadv.aar4740>

695 Chatanantavet, P., & Lamb, M. P. (2014). Sediment transport and topographic evolution of a coupled
696 river and river plume system: An experimental and numerical study: EXPERIMENTS COUPLED RIVER &
697 RIVER-PLUME. *Journal of Geophysical Research: Earth Surface*, 119(6), 1263–1282.
698 <https://doi.org/10.1002/2013JF002810>

699 Chatanantavet, P., Lamb, M. P., & Nittrouer, J. A. (2012). Backwater controls of avulsion location on
700 deltas. *Geophysical Research Letters*, 39(1), 2011GL050197. <https://doi.org/10.1029/2011GL050197>

701 Chen, C., Tian, B., Schwarz, C., Zhang, C., Guo, L., Xu, F., Zhou, Y., & He, Q. (2021). Quantifying delta
702 channel network changes with Landsat time-series data. *Journal of Hydrology*, 600, 126688.
703 <https://doi.org/10.1016/j.jhydrol.2021.126688>

704 Coffey, T. S., & Shaw, J. B. (2017). Congruent Bifurcation Angles in River Delta and Tributary Channel
705 Networks. *Geophysical Research Letters*, 44(22). <https://doi.org/10.1002/2017GL074873>

706 Davidson, S. K., & Hartley, A. J. (2014). A Quantitative Approach To Linking Drainage Area and
707 Distributive-Fluvial-System Area In Modern and Ancient Endorheic Basins. *Journal of Sedimentary*
708 *Research*, 84(11), 1005–1020. <https://doi.org/10.2110/jsr.2014.79>

709 Davidson, S. K., Hartley, A. J., Weissmann, G. S., Nichols, G. J., & Scuderi, L. A. (2013). Geomorphic
710 elements on modern distributive fluvial systems. *Geomorphology*, 180–181, 82–95.
711 <https://doi.org/10.1016/j.geomorph.2012.09.008>

712 De Toffoli, B., Plesa, A. -C., Hauber, E., & Breuer, D. (2021). Delta Deposits on Mars: A Global Perspective.
713 *Geophysical Research Letters*, 48(17), e2021GL094271. <https://doi.org/10.1029/2021GL094271>

714 Devauchelle, O., Petroff, A. P., Seybold, H. F., & Rothman, D. H. (2012). Ramification of stream networks.
715 *Proceedings of the National Academy of Sciences*, 109(51), 20832–20836.
716 <https://doi.org/10.1073/pnas.1215218109>

717 Di Achille, G., & Hynes, B. M. (2010). Ancient ocean on Mars supported by global distribution of deltas
718 and valleys. *Nature Geoscience*, 3(7), 459–463. <https://doi.org/10.1038/ngeo891>

719 Dong, T. Y., Nittrouer, J. A., Il'icheva, E., Pavlov, M., McElroy, B., Czapiga, M. J., Ma, H., & Parker, G.
720 (2016). Controls on gravel termination in seven distributary channels of the Selenga River Delta, Baikal
721 Rift basin, Russia. *Geological Society of America Bulletin*, 128(7–8), 1297–1312.
722 <https://doi.org/10.1130/B31427.1>

723 Donselaar, M. E., Cuevas Gozalo, M. C., & Moyano, S. (2013). Avulsion processes at the terminus of low-
724 gradient semi-arid fluvial systems: Lessons from the Río Colorado, Altiplano endorheic basin, Bolivia.
725 *Sedimentary Geology*, 283, 1–14. <https://doi.org/10.1016/j.sedgeo.2012.10.007>

726 Edmonds, D. A., Martin, H. K., Valenza, J. M., Henson, R., Weissmann, G. S., Miltenberger, K., Mans, W.,
727 Moore, J. R., Slingerland, R. L., Gibling, M. R., Bryk, A. B., & Hajek, E. A. (2022). Rivers in reverse:
728 Upstream-migrating dechannelization and flooding cause avulsions on fluvial fans. *Geology*, 50(1), 37–
729 41. <https://doi.org/10.1130/G49318.1>

730 Edmonds, D. A., Paola, C., Hoyal, D. C. J. D., & Sheets, B. A. (2011). Quantitative metrics that describe
731 river deltas and their channel networks. *Journal of Geophysical Research*, 116(F4), F04022.
732 <https://doi.org/10.1029/2010JF001955>

733 Edmonds, D. A., & Slingerland, R. L. (2007). Mechanics of river mouth bar formation: Implications for the
734 morphodynamics of delta distributary networks. *Journal of Geophysical Research: Earth Surface*,
735 112(F2), 2006JF000574. <https://doi.org/10.1029/2006JF000574>

736 ESRI. (2025). *World Imagery* [Imagery layer]. Esri, Maxar.
737 <https://www.arcgis.com/home/item.html?id=10df2279f9684e4a9f6a7f08febac2a9>

738 Fagherazzi, S. (2008). Self-organization of tidal deltas. *Proceedings of the National Academy of Sciences*,
739 105(48), 18692–18695. <https://doi.org/10.1073/pnas.0806668105>

740 Fagherazzi, S., Edmonds, D. A., Nardin, W., Leonardi, N., Canestrelli, A., Falcini, F., Jerolmack, D. J.,
741 Mariotti, G., Rowland, J. C., & Slingerland, R. L. (2015). Dynamics of river mouth deposits. *Reviews of*
742 *Geophysics*, 53(3), 642–672. <https://doi.org/10.1002/2014RG000451>

743 Farley, K. A., Williford, K. H., Stack, K. M., Bhartia, R., Chen, A., De La Torre, M., Hand, K., Goreva, Y.,
744 Herd, C. D. K., Hueso, R., Liu, Y., Maki, J. N., Martinez, G., Moeller, R. C., Nelessen, A., Newman, C. E.,
745 Nunes, D., Ponce, A., Spanovich, N., ... Wiens, R. C. (2020). Mars 2020 Mission Overview. *Space Science*
746 *Reviews*, 216(8), 142. <https://doi.org/10.1007/s11214-020-00762-y>

747 Federici, B., & Paola, C. (2003). Dynamics of channel bifurcations in noncohesive sediments. *Water*
748 *Resources Research*, 39(6), 2002WR001434. <https://doi.org/10.1029/2002WR001434>

749 Fielding, C. R., Ashworth, P. J., Best, J. L., Prokocki, E. W., & Smith, G. H. S. (2012). Tributary, distributary
750 and other fluvial patterns: What really represents the norm in the continental rock record? *Sedimentary*
751 *Geology*, 261–262, 15–32. <https://doi.org/10.1016/j.sedgeo.2012.03.004>

752 Fontana, A., Mozzi, P., & Marchetti, M. (2014). Alluvial fans and megafans along the southern side of the
753 Alps. *Sedimentary Geology*, 301, 150–171. <https://doi.org/10.1016/j.sedgeo.2013.09.003>

754 Friend, P. F. (1978). *DISTINCTIVE FEATURES OF SOME ANCIENT RIVER SYSTEMS*.

755 Galloway, E. (1975). Process Framework for Describing the Morphologic and Stratigraphic Evolution of
756 Deltaic Depositional Systems. *Deltas: Models for Exploration*, 1975, 87–98.

757 Ganti, V., Chu, Z., Lamb, M. P., Nittrouer, J. A., & Parker, G. (2014). Testing morphodynamic controls on
758 the location and frequency of river avulsions on fans versus deltas: Huanghe (Yellow River), China.
759 *Geophysical Research Letters*, 41(22), 7882–7890. <https://doi.org/10.1002/2014GL061918>

760 Gearon, J. H., Martin, H. K., DeLisle, C., Barefoot, E. A., Mohrig, D., Paola, C., & Edmonds, D. A. (2024).
761 Rules of river avulsion change downstream. *Nature*, 634(8032), 91–95. [https://doi.org/10.1038/s41586-](https://doi.org/10.1038/s41586-024-07964-2)
762 [024-07964-2](https://doi.org/10.1038/s41586-024-07964-2)

763 Geleynse, N., Storms, J. E. A., Walstra, D.-J. R., Jagers, H. R. A., Wang, Z. B., & Stive, M. J. F. (2011).
764 Controls on river delta formation; insights from numerical modelling. *Earth and Planetary Science*
765 *Letters*, 302(1–2), 217–226. <https://doi.org/10.1016/j.epsl.2010.12.013>

766 Giosan, L., Syvitski, J., Constantinescu, S., & Day, J. (2014). Climate change: Protect the world's deltas.
767 *Nature*, 516(7529), 31–33. <https://doi.org/10.1038/516031a>

768 Hansford, M. R., & Plink-Björklund, P. (2020). River discharge variability as the link between climate and
769 fluvial fan formation. *Geology*, 48(10), 952–956. <https://doi.org/10.1130/G47471.1>

770 Hariharan, J., Piliouras, A., Schwenk, J., & Passalacqua, P. (2022). Width-Based Discharge Partitioning in
771 Distributary Networks: How Right We Are. *Geophysical Research Letters*, 49(14), e2022GL097897.
772 <https://doi.org/10.1029/2022GL097897>

773 Harris, C. R., Millman, K. J., van der Walt, S. J., Gommers, R., Virtanen, P., Cournapeau, D., Wieser, E.,
774 Taylor, J., Berg, S., Smith, N. J., Kern, R., Picus, M., Hoyer, S., van Kerkwijk, M. H., Brett, M., Haldane, A.,
775 del Río, J. F., Wiebe, M., Peterson, P., ... Oliphant, T. E. (2020). Array programming with NumPy. *Nature*,
776 585(7825), 357–362. <https://doi.org/10.1038/s41586-020-2649-2>

777 Hartley, A. J., Weissmann, G. S., Nichols, G. J., & Warwick, G. L. (2010). Large Distributive Fluvial Systems:
778 Characteristics, Distribution, and Controls on Development. *Journal of Sedimentary Research*, 80(2),
779 167–183. <https://doi.org/10.2110/jsr.2010.016>

780 Horton, B. K., & Decelles, P. G. (2001). *Modern and ancient Fluvial megafans in the foreland basin system*
781 *of the central Andes, southern Bolivia: Implications for drainage network evolution in fold-thrust belts*
782 (pp. 43–63).

783 Hunter, J. D. (2007). MATPLOTLIB - 2D GRAPHICS ENVIRONMENT. *Computing in Science & Engineering*.

784 Isikdogan, F., Bovik, A., & Passalacqua, P. (2017). RivaMap: An automated river analysis and mapping
785 engine. *Remote Sensing of Environment*, 202, 88–97. <https://doi.org/10.1016/j.rse.2017.03.044>

786 Jerolmack, D. J. (2009). Conceptual framework for assessing the response of delta channel networks to
787 Holocene sea level rise. *Quaternary Science Reviews*, 28(17–18), 1786–1800.
788 <https://doi.org/10.1016/j.quascirev.2009.02.015>

789 Jerolmack, D. J., & Swenson, J. B. (2007). Scaling relationships and evolution of distributary networks on
790 wave-influenced deltas. *Geophysical Research Letters*, 34(23), 2007GL031823.
791 <https://doi.org/10.1029/2007GL031823>

792 Jones, L. S., & Schumm, S. A. (1999). Causes of Avulsion: An Overview. In N. D. Smith & J. Rogers (Eds.),
793 *Fluvial Sedimentology VI* (1st ed., pp. 169–178). Wiley. <https://doi.org/10.1002/9781444304213.ch13>

794 Ke, W., Shaw, J. B., Mahon, R. C., & Cathcart, C. A. (2019). Distributary Channel Networks as Moving
795 Boundaries: Causes and Morphodynamic Effects. *Journal of Geophysical Research: Earth Surface*, 124(7),
796 1878–1898. <https://doi.org/10.1029/2019JF005084>

797 Kelly, S. B., & Olsen, H. (1993). Terminal fans a review with reference to Devonian examples. In
798 *Sedimentary Geology* (Vol. 85, pp. 339–374).

799 Lauzon, R., Piliouras, A., & Rowland, J. C. (2019). Ice and Permafrost Effects on Delta Morphology and
800 Channel Dynamics. *Geophysical Research Letters*, 46(12), 6574–6582.
801 <https://doi.org/10.1029/2019GL082792>

802 Leier, A. L., DeCelles, P. G., & Pelletier, J. D. (2005). Mountains, monsoons, and megafans. *Geology*,
803 33(4), 289. <https://doi.org/10.1130/G21228.1>

804 Leonardi, N., Canestrelli, A., Sun, T., & Fagherazzi, S. (2013). Effect of tides on mouth bar morphology
805 and hydrodynamics. *Journal of Geophysical Research: Oceans*, 118(9), 4169–4183.
806 <https://doi.org/10.1002/jgrc.20302>

807 Limaye, A. B., Adler, J. B., Moodie, A. J., Whipple, K. X., & Howard, A. D. (2023). Effect of Standing Water
808 on Formation of Fan-Shaped Sedimentary Deposits at Hypanis Valles, Mars. *Geophysical Research*
809 *Letters*, 50(4), e2022GL102367. <https://doi.org/10.1029/2022GL102367>

810 Mahon, R., Hughes, C., Chen, H., & Shaw, J. (2024). Ancient Channel-Mouth Bifurcation Angles on Earth
811 and Mars. *The Sedimentary Record*, 22(1). <https://doi.org/10.2110/001c.124824>

812 Malin, M. C., & Edgett, K. S. (2015). *Evidence for Persistent Flow and Aqueous Sedimentation on Early*
813 *Mars*. www.sciencemag.org

814 Martin, H. K., & Edmonds, D. A. (2023). Avulsion dynamics determine fluvial fan morphology in a cellular
815 model. *Geology*, 51(8), 796–800. <https://doi.org/10.1130/G51138.1>

- 816 Mendenhall, W., Beaver, R. J., & Beaver, B. M. (2012). *Introduction to Probability and Statistics*.
817 Brooks/Cole.
- 818 Mohrig, D., Heller, P. L., Paola, C., & Lyons, W. J. (2000). Interpreting avulsion process from ancient
819 alluvial sequences: Guadalupe-Matarranya system (northern Spain) and Wasatch Formation (western
820 Colorado). *Geological Society of America Bulletin*.
- 821 Morais, E. S., & Montanher, O. C. (2022). Avulsion in a meandering river: Floodplain conditions for
822 occurrence and effects in the parent channel. *CATENA*, 214, 106236.
823 <https://doi.org/10.1016/j.catena.2022.106236>
- 824 Morón, S., Amos, K., Edmonds, D. A., Payenberg, T., Sun, X., & Thyer, M. (2017). Avulsion triggering by El
825 Niño–Southern Oscillation and tectonic forcing: The case of the tropical Magdalena River, Colombia. *GSA
826 Bulletin*, 129(9–10), 1300–1313. <https://doi.org/10.1130/B31580.1>
- 827 Moscariello, A. (2018). Alluvial fans and fluvial fans at the margins of continental sedimentary basins:
828 Geomorphic and sedimentological distinction for geo-energy exploration and development. *Geological
829 Society, London, Special Publications*, 440(1), 215–243. <https://doi.org/10.1144/SP440.11>
- 830 Nichols, G. J. (1987). *STRUCTURAL CONTROLS ON FLUVIAL DISTRIBUTARY SYSTEMS-THE LUNA SYSTEM,
831 NORTHERN SPAIN*.
- 832 Nichols, G. J., & Fisher, J. A. (2007). Processes, facies and architecture of fluvial distributary system
833 deposits. *Sedimentary Geology*, 195(1–2), 75–90. <https://doi.org/10.1016/j.sedgeo.2006.07.004>
- 834 Nienhuis, J. H., Ashton, A. D., Edmonds, D. A., Hoitink, A. J. F., Kettner, A. J., Rowland, J. C., & Törnqvist,
835 T. E. (2020). Global-scale human impact on delta morphology has led to net land area gain. *Nature*,
836 577(7791), 514–518. <https://doi.org/10.1038/s41586-019-1905-9>
- 837 Nienhuis, J. H., Ashton, A. D., & Giosan, L. (2015). What makes a delta wave-dominated? *Geology*, 43(6),
838 511–514. <https://doi.org/10.1130/G36518.1>
- 839 Nienhuis, J. H., Hoitink, A. J. F. T., & Törnqvist, T. E. (2018). Future Change to Tide-Influenced Deltas.
840 *Geophysical Research Letters*, 45(8), 3499–3507. <https://doi.org/10.1029/2018GL077638>
- 841 North, C. P., & Warwick, G. L. (2007). Fluvial Fans: Myths, Misconceptions, and the End of the Terminal-
842 Fan Model. *Journal of Sedimentary Research*, 77(9), 693–701. <https://doi.org/10.2110/jsr.2007.072>
- 843 Olariu, C., & Bhattacharya, J. P. (2006). Terminal distributary channels and delta front architecture of
844 river-dominated delta systems. *Journal of Sedimentary Research*, 76(2), 212–233.
845 <https://doi.org/10.2110/jsr.2006.026>
- 846 Ori, G. G., Marinangeli, L., & Baliva, A. (2000). Terraces and Gilbert-type deltas in crater lakes in Ismenius
847 Lacus and Memnonia (Mars). *Journal of Geophysical Research: Planets*, 105(E7), 17629–17641.
848 <https://doi.org/10.1029/1999JE001219>
- 849 Owen, A., Nichols, G. J., Hartley, A. J., Weissmann, G. S., & Scuderi, L. A. (2015). Quantification of a
850 Distributive Fluvial System: The Salt Wash DFS of the Morrison Formation, SW U.S.A. *Journal of
851 Sedimentary Research*, 85(5), 544–561. <https://doi.org/10.2110/jsr.2015.35>

852 Paniagua-Arroyave, J. F., & Nienhuis, J. H. (2024). The Quantified Galloway Ternary Diagram of Delta
853 Morphology. *Journal of Geophysical Research: Earth Surface*, 129(11), e2024JF007878.
854 <https://doi.org/10.1029/2024JF007878>

855 Paola, C., Twilley, R. R., Edmonds, D. A., Kim, W., Mohrig, D., Parker, G., Viparelli, E., & Voller, V. R.
856 (2011). Natural Processes in Delta Restoration: Application to the Mississippi Delta. *Annual Review of*
857 *Marine Science*, 3(1), 67–91. <https://doi.org/10.1146/annurev-marine-120709-142856>

858 Parker, G., Paola, C., Whipple, K. X., & Mohrig, D. (1998). ALLUVIAL FANS FORMED BY CHANNELIZED
859 FLUVIAL AND SHEET FLOW. I: THEORY. *Journral OF Hydraulic Engineering*, 985–995.

860 Passalacqua, P. (2017). The Delta Connectome: A network-based framework for studying connectivity in
861 river deltas. *Geomorphology*, 277, 50–62. <https://doi.org/10.1016/j.geomorph.2016.04.001>

862 Pearson, S. G., Van Prooijen, B. C., Elias, E. P. L., Vitousek, S., & Wang, Z. B. (2020). Sediment
863 Connectivity: A Framework for Analyzing Coastal Sediment Transport Pathways. *Journal of Geophysical*
864 *Research: Earth Surface*, 125(10), e2020JF005595. <https://doi.org/10.1029/2020JF005595>

865 Piliouras, A., Lauzon, R., & Rowland, J. C. (2021). Unraveling the Combined Effects of Ice and Permafrost
866 on Arctic Delta Morphodynamics. *Journal of Geophysical Research: Earth Surface*, 126(4),
867 e2020JF005706. <https://doi.org/10.1029/2020JF005706>

868 Pizzuto, J. E. (1987). Sediment diffusion during overbank flows. *Sedimentology*, 34(2), 301–317.
869 <https://doi.org/10.1111/j.1365-3091.1987.tb00779.x>

870 Plink-Björklund, P. (2021). Distributive Fluvial Systems: Fluvial and Alluvial Fans. In *Encyclopedia of*
871 *Geology* (pp. 745–758). Elsevier. <https://doi.org/10.1016/B978-0-08-102908-4.00015-1>

872 Radebaugh, J., Ventra, D., Lorenz, R. D., Farr, T., Kirk, R., Hayes, A., Malaska, M. J., Birch, S., Liu, Z. Y.-C.,
873 Lunine, J., Barnes, J., Le Gall, A., Lopes, R., Stofan, E., Wall, S., & Paillou, P. (2018). Alluvial and fluvial fans
874 on Saturn’s moon Titan reveal processes, materials and regional geology. *Geological Society, London,*
875 *Special Publications*, 440(1), 281–305. <https://doi.org/10.1144/SP440.6>

876 Rahman, M. M., Howell, J. A., & MacDonald, D. I. M. (2022). Quantitative analysis of crevasse-splay
877 systems from modern fluvial settings. *Journal of Sedimentary Research*, 92(9), 751–774.
878 <https://doi.org/10.2110/jsr.2020.067>

879 Reitz, M. D., & Jerolmack, D. J. (2012). Experimental alluvial fan evolution: Channel dynamics, slope
880 controls, and shoreline growth. *Journal of Geophysical Research: Earth Surface*, 117(F2), 2011JF002261.
881 <https://doi.org/10.1029/2011JF002261>

882 Saito, Y., Thanawat, J., Chaimanee, N., Jarupongsakul, T., & Syvitski, J. P. M. (2007). *Shrinking*
883 *Megadeltas in Asia: Sea-level Rise and Sediment Reduction Impacts from Case Study of the Chao Phraya*
884 *Delta The Holocene Red River Delta, Vietnam View project Global Risks and research priorities for coastal*
885 *subsidence View project Shrinking Megadeltas in Asia: Sea-level Rise and Sediment Reduction Impacts*
886 *from Case Study of the Chao Phraya Delta*. <https://www.researchgate.net/publication/234045413>

887 Schumm, S. A. (1977). The fluvial system. *Food and Agriculture Organization of the United Nations*.

- 888 Schwanghart, W., & Kuhn, N. J. (2010). TopoToolbox: A set of Matlab functions for topographic analysis.
889 *Environmental Modelling & Software*, 25(6), 770–781. <https://doi.org/10.1016/j.envsoft.2009.12.002>
- 890 Seybold, H., Andrade, J. S., & Herrmann, H. J. (2007). Modeling river delta formation. *Proceedings of the*
891 *National Academy of Sciences*, 104(43), 16804–16809. <https://doi.org/10.1073/pnas.0705265104>
- 892 Seybold, H. J., Kite, E., & Kirchner, J. W. (2018). Branching geometry of valley networks on Mars and
893 Earth and its implications for early Martian climate. *Science Advances*, 4(6), eaar6692.
894 <https://doi.org/10.1126/sciadv.aar6692>
- 895 Seybold, H., Rothman, D. H., & Kirchner, J. W. (2017). Climate’s watermark in the geometry of stream
896 networks. *Geophysical Research Letters*, 44(5), 2272–2280. <https://doi.org/10.1002/2016GL072089>
- 897 Shaw, J. B., Miller, K., & McElroy, B. (2018). Island Formation Resulting From Radially Symmetric Flow
898 Expansion. *Journal of Geophysical Research: Earth Surface*, 123(2), 363–383.
899 <https://doi.org/10.1002/2017JF004464>
- 900 Singh, H., Parkash, B., & Gohain, K. (1993). Facies analysis of the Kosi megafan deposits. *Sedimentary*
901 *Geology*, 85(1–4), 87–113. [https://doi.org/10.1016/0037-0738\(93\)90077-I](https://doi.org/10.1016/0037-0738(93)90077-I)
- 902 Sinha, R. (2009). The Great avulsion of Kosi on 18 August 2008. *Current Science*, 97(3), 429–433.
- 903 Slingerland, R., & Smith, N. D. (1998). Necessary conditions for a meandering-river avulsion. *Geology*,
904 26(5), 435. [https://doi.org/10.1130/0091-7613\(1998\)026%253C0435:NCFAMR%253E2.3.CO;2](https://doi.org/10.1130/0091-7613(1998)026%253C0435:NCFAMR%253E2.3.CO;2)
- 905 Slingerland, R., & Smith, N. D. (2004). RIVER AVULSIONS AND THEIR DEPOSITS. *Annual Review of Earth*
906 *and Planetary Sciences*, 32(1), 257–285. <https://doi.org/10.1146/annurev.earth.32.101802.120201>
- 907 Smart, J. S. (1971). *QUANTITATIVE PROPERTIES OF DELTA CHANNEL NETWORKS*.
- 908 Syvitski, J. P. M., & Brakenridge, G. R. (2013). Causation and avoidance of catastrophic flooding along the
909 Indus River, Pakistan. *GSA Today*, 23(1), 4–10. <https://doi.org/10.1130/GSATG165A.1>
- 910 Syvitski, J. P. M., Kettner, A. J., Overeem, I., Hutton, E. W. H., Hannon, M. T., Brakenridge, G. R., Day, J.,
911 Vörösmarty, C., Saito, Y., Giosan, L., & Nicholls, R. J. (2009). Sinking deltas due to human activities.
912 *Nature Geoscience*, 2(10), 681–686. <https://doi.org/10.1038/ngeo629>
- 913 Tebolt, M., & Goudge, T. A. (2022). Global investigation of martian sedimentary fan features: Using
914 stratigraphic analysis to study depositional environment. *Icarus*, 372, 114718.
915 <https://doi.org/10.1016/j.icarus.2021.114718>
- 916 Tejedor, A., Longjas, A., Edmonds, D. A., Zaliapin, I., Georgiou, T. T., Rinaldo, A., & Foufoula-Georgiou, E.
917 (2017). Entropy and optimality in river deltas. *Proceedings of the National Academy of Sciences*, 114(44),
918 11651–11656. <https://doi.org/10.1073/pnas.1708404114>
- 919 Tejedor, A., Longjas, A., Zaliapin, I., & Foufoula-Georgiou, E. (2015). Delta channel networks: 1. A graph-
920 theoretic approach for studying connectivity and steady state transport on deltaic surfaces. *Water*
921 *Resources Research*, 51(6), 3998–4018. <https://doi.org/10.1002/2014WR016577>
- 922 Törnqvist, T. E., & Bridge, J. S. (2002). Spatial variation of overbank aggradation rate and its influence on
923 avulsion frequency. *Sedimentology*, 49(5), 891–905. <https://doi.org/10.1046/j.1365-3091.2002.00478.x>

924 Trampush, S. M., & Hajek, E. A. (2017). Preserving proxy records in dynamic landscapes: Modeling and
925 examples from the Paleocene-Eocene Thermal Maximum. *Geology*, *45*(11), 967–970.
926 <https://doi.org/10.1130/G39367.1>

927 Trauth, M. H. (2006). *MATLAB® Recipes for Earth Sciences*.

928 Ventra, D., & Clarke, L. E. (2018). Geology and geomorphology of alluvial and fluvial fans: Current
929 progress and research perspectives. *Geological Society, London, Special Publications*, *440*(1), 1–21.
930 <https://doi.org/10.1144/SP440.16>

931 Virtanen, P., Gommers, R., Oliphant, T. E., Haberland, M., Reddy, T., Cournapeau, D., Burovski, E.,
932 Peterson, P., Weckesser, W., Bright, J., van der Walt, S. J., Brett, M., Wilson, J., Millman, K. J., Mayorov,
933 N., Nelson, A. R. J., Jones, E., Kern, R., Larson, E., ... Vázquez-Baeza, Y. (2020). SciPy 1.0: Fundamental
934 algorithms for scientific computing in Python. *Nature Methods*, *17*(3), 261–272.
935 <https://doi.org/10.1038/s41592-019-0686-2>

936 Vulis, L., Tejedor, A., Ma, H., Nienhuis, J. H., Broaddus, C. M., Brown, J., Edmonds, D. A., Rowland, J. C., &
937 Fofoula-Georgiou, E. (2023). River Delta Morphotypes Emerge From Multiscale Characterization of
938 Shorelines. *Geophysical Research Letters*, *50*(7), e2022GL102684.
939 <https://doi.org/10.1029/2022GL102684>

940 Walker, H. J. (1998). Arctic Deltas. *Journal of Coastal Research*, *14*(3), 718–738.

941 Wall, S., Hayes, A., Bristow, C., Lorenz, R., Stofan, E., Lunine, J., Le Gall, A., Janssen, M., Lopes, R., Wye,
942 L., Soderblom, L., Paillou, P., Aharonson, O., Zebker, H., Farr, T., Mitri, G., Kirk, R., Mitchell, K.,
943 Notarnicola, C., ... Ventura, B. (2010). Active shoreline of Ontario Lacus, Titan: A morphological study of
944 the lake and its surroundings. *Geophysical Research Letters*, *37*(5), 2009GL041821.
945 <https://doi.org/10.1029/2009GL041821>

946 Wang, J., & Plink-Björklund, P. (2019). Stratigraphic complexity in fluvial fans: Lower Eocene Green River
947 Formation, Uinta Basin, USA. *Basin Research*, *31*(5), 892–919. <https://doi.org/10.1111/bre.12350>

948 Waskom, M. (2021). seaborn: Statistical data visualization. *Journal of Open Source Software*, *6*(60), 3021.
949 <https://doi.org/10.21105/joss.03021>

950 Weissman, G. S., Hartley, A. J., Nichols, G. J., Scuderi, L. A., Olson, M., Buehler, H., & Banteah, R. (2010).
951 *Fluvial form in modern continental sedimentary basins: Distributive fluvial systems*.
952 <https://doi.org/10.1016/j.geo>

953 Weissmann, G. S., Hartley, A. J., Nichols, G. J., Scuderi, L. A., Olson, M., Buehler, H., & Banteah, R. (2010).
954 Fluvial form in modern continental sedimentary basins: Distributive fluvial systems. *Geology*, *38*(1), 39–
955 42. <https://doi.org/10.1130/G30242.1>

956 Weissmann, G. S., Hartley, A. J., Scuderi, L. A., Nichols, G. J., Owen, A., Wright, S., Felicia, A. L., Holland,
957 F., & Anaya, F. M. L. (2015). Fluvial geomorphic elements in modern sedimentary basins and their
958 potential preservation in the rock record: A review. *Geomorphology*, *250*, 187–219.
959 <https://doi.org/10.1016/j.geomorph.2015.09.005>

960 Witek, P. P., & Czechowski, L. (2015). Dynamical modelling of river deltas on Titan and Earth. *Planetary
961 and Space Science*, *105*, 65–79. <https://doi.org/10.1016/j.pss.2014.11.005>

962 Wolinsky, M. A., Edmonds, D. A., Martin, J., & Paola, C. (2010). Delta allometry: Growth laws for river
963 deltas. *Geophysical Research Letters*, 37(21), 2010GL044592. <https://doi.org/10.1029/2010GL044592>

964 Wood, L. J. (2006). Quantitative geomorphology of the Mars Eberswalde delta. *Geological Society of
965 America Bulletin*, 118(5–6), 557–566. <https://doi.org/10.1130/B25822.1>

966 Wright, L. D. (1977). Sediment transport and deposition at river mouths: A synthesis. *Geological Society
967 of America Bulletin*, 88(6), 857. [https://doi.org/10.1130/0016-
968 7606\(1977\)88%253C857:STADAR%253E2.0.CO;2](https://doi.org/10.1130/0016-7606(1977)88%253C857:STADAR%253E2.0.CO;2)

969 Xu, Z., & Plink-Björklund, P. (2023). Quantifying Formative Processes in River- and Tide-Dominated
970 Deltas for Accurate Prediction of Future Change. *Geophysical Research Letters*, 50(20), e2023GL104434.
971 <https://doi.org/10.1029/2023GL104434>

972 Yang, H. (2020). Numerical investigation of avulsions in gravel-bed braided rivers. *Hydrological
973 Processes*, 34(17), 3702–3717. <https://doi.org/10.1002/hyp.13837>

974